C.P. No. 924

MINISTRY OF TECHNOLOGY

AERONAUTICAL RESEARCH COUNCIL

CURRENT PAPERS

Camber Effects on the Non-Linear Lift of Slender Wings with Sharp Leading Edges

By

L. C. Squire,
Engineering Laboratory,
University of Cambridge

LONDON: HER MAJESTY'S STATIONERY OFFICE
1967
SEVEN SHILLINGS NET

C.P. No. 924*

January, 1966

Camber Effects on the Non-linear Lift of Slender Wings with Sharp Leading Edges

by

L. C. Squire

Engineering Laboratory, University of Cambridge

Summary

A study of published work on slender wings has shown that the non-linear lift is often increased by leading edge droop. In this note the results are given of an investigation, made on simple, conically cambered wings, to study this effect in more detail. It is found that the main parameter which determines the increase in non-linear lift is the angle of droop at the leading edge. The magnitude of the increase, and the corresponding movements of the vortex positions, are predicted qualitatively by a simple extension to the Brown & Michael theory carried out for conically cambered wings with circular arc cross-sections. A study of the theoretical results shows that the principal cause of the increase in lift is the distortion of the velocity field of the vorticity which is produced by the curvature of the wing in the cross-flow plane.

---

*Replaces A.R.C.27 651

1. Introduction

The main features of the flow over slender wings at incidence are now well understood. Basically the flow separates from the leading edges to form a pair of free vortex sheets which roll up into a pair of contra-rotating vortices above the wing surface. Associated with these vortices there is a suction peak inboard of each leading edge on the wing's upper surface. The suction peaks give an increase in lift-curve slope with increase in incidence and so cause the characteristic non-linear lift curves of slender wings. This paper is concerned with the effects of leading edge droop on the non-linear lift development.

These effects first became apparent in wind-tunnel tests on early models of a supersonic transport aircraft; the models were slender wings of different planforms and incorporated various types of leading edge droop to meet certain design requirements in the supersonic cruising condition, (see, for example, Ref. 1). The main effects are illustrated in Figs. 1 and 2 by data from Refs. 2, 3 and 4. Fig. 1 refers to cambered gothic wings of aspect ratio 0.75, full details of which can be found in Refs. 2 and 3. The inner parts of these wings were plane and the outer parts, near the leading edges, were drooped to give attached flow at a given design lift coefficient. The amount of droop was greater the higher the design lift coefficient. The droop was greatest at about halfway along the leading edge and fell to zero at the trailing edge.

The left-hand graph of Fig. 1 shows the development of lift with the incidence of the central plane portion of the wings. All the wings show the characteristic non-linear lift curves of slender wings, but the point of minimum lift-curve slope occurs at positive incidence on the cambered wings. However, the results for the wing with a design lift coefficient of 0.05 show that although the minimum lift-curve slope occurs at about $4°$ ($C_L = 0.07$), when the actual lift is lower than that of the plane wing, yet by $\alpha = 18°$ the lift of this cambered wing has caught up that of the plane wing. This effect is analysed in more detail in the two right-hand figures. The upper graph shows the ratio of the increment of lift for neighbouring measured points to the corresponding increment in incidence, plotted against incidence. The curves for all three wings have a flat 'V' shape with a clearly defined apex. This apex corresponds to the incidence for minimum lift-curve slope and the incidence for attached flow at the leading edge. (The fact that the minimum lift-curve slope occurs at the condition of flow attachment has been confirmed by numerous oil flow tests; see for example Ref. 4). The three curves are replotted in the lower figure against incidence away from the attachment incidence. This figure shows that the cambered wings have a larger minimum lift-curve slope than the plane wing, and that away from the attachment point the increase in lift-curve slope is greater than on the plane wing, i.e. at a given incidence above the attachment point the camber results in a greater non-linear lift.

These effects are further illustrated in Fig. 2 where lift-curve slopes are plotted against $(\alpha - \bar{\alpha})$ for the plane wing and three cambered wings for which results are given in Ref. 4. The camber of these wings is more complicated than that of the wings in Fig. 1, but all have drooped leading edges. Again the cambered wings have more non-linear lift than the plane wing. This is true throughout the tested Mach number range $(0.4 \leqslant M \leqslant 2.0)$ and is in fact most marked at the highest speeds where the lift of the plane wing is tending to become linear.

In this paper these effects are studied in more detail by means of theoretical and low-speed experimental investigations of the non-linear lift development on a series of simple models with conical camber.

2. Details of the Experimental Programme

Details of the seven wings tested in the main experimental investigation are shown in Figs. 3(a) and 3(b). All the wings were straight deltas of aspect ratio 1.0, with an overall length of 40 inches. The centre portions of the wings were approximately 0.5 inch thick and the leading edges were tapered on the upper surface to give a sharp edge with an included angle of approximately 14° normal to the edge. For the basic models the trailing edge was cut off square, but some tests were made on the flat wing with a sharp trailing edge. The sharp edge was obtained by a bevel on the upper surface, giving a trailing edge angle of 12°.

The cambered models are defined in terms of the shape of their lower surfaces with approximately the same thickness distribution as for the flat wing added above this surface. The equations of the camber surfaces are given by

$$\frac{z}{\epsilon x} = -\beta\left(\frac{y}{\epsilon x}\right)^n ,$$

where β and n are constants for a given wing, and where x is measured along the wing chord, y spanwise and z vertically upwards from the apex. ϵ is the tangent of the semi-angle of the apex of the planform, i.e. it is the ratio of the semi-span to the root-chord. The droop of the leading edge relative to the centre line is thus β and the leading edge droop angle is $\tan^{-1}(n\beta)$. Values of n and β for the various wings are given in Table I.

Table I

Wing	n	β	ϕ (leading edge droop angle $= \tan^{-1} n\beta$)
2	2	0.15	16.7°
3	5	0.15	36.8°
4	1	0.30	16.7°
5	3	0.30	42.0°
6	5	0.30	56.3°
7	7	0.30	64.5°

From this Table it can be seen that:

(i) wings 2 and 4 have the same droop angles but different total droop at the leading edge,

(ii) wing 3 has the same camber equation, but half as much overall droop as wing 6; also it has slightly less leading edge droop angle than wing 4, but only half as much total droop at the leading edge,

(iii) wings 4 to 7 have the same total droop at the leading edge, but give a wide range of leading edge droop angles.

All the models were tested in the $5\frac{1}{2}$ ft x 4 ft low-speed wind tunnel in the Engineering Laboratory at Cambridge University. Overall force tests and surface oil flow tests were made at a speed of 100 ft/sec or a Reynolds number of 1.6×10^6 based on mean chord. Lift, drag and pitching moment was measured for an incidence range up to about 20°, with the models wire-mounted on a mechanical balance. The results have been corrected for tunnel interference by the methods given in Ref. 5 and the estimated accuracy is as follows:

$$\alpha \quad \mp 0.1°$$

$$C_L \quad \pm 0.003$$

$$C_m \quad \pm 0.002$$

$$C_D \quad \pm 0.0005.$$

Pitching moments are quoted about the quarter-chord point of the aerodynamic mean chord.

Surface oil flow patterns were obtained by using a paint composed of titanium dioxide in a mixture of paraffin (Kerosene) and linseed oil.

The vertical positions of the vortices were measured by injecting a streamer of smoke into the tunnel upstream of the model

and adjusting the position of the smoke source until the vortex core was visible. The vertical position was then measured by sighting across reference marks on the sides of the tunnel. Accurate measurement was not possible when the vortex lay below the wing centre line (see Fig. 9). These smoke tests were made at about 20 ft sec.

All the basic tests were made with natural transition on the wing.

3. Experimental Results

3.1 Flat wing results

Lift results for the flat wing with a bluff trailing edge and a bevelled trailing edge are presented in Figs. 4 and 5. Except for a displacement in α for $C_L = 0$ the lift curves for the two trailing edge shapes are similar in shape. However, the curves of $\Delta C_L / \Delta \alpha$ (Fig. 5) show that the minimum lift-curve slope occurs at a slightly higher incidence with the bluff trailing edge (1.3° compared with 0.7°). The differences are, however, small and are probably associated with the fact that the bevelled trailing edge effectively produces a small camber. In the lower two figures of Fig. 5 $\Delta C_L / \Delta \alpha$ is replotted against $(\alpha - \bar{\alpha})$; in both figures the dashed symbols are for the flat suction surface. For the wing with a bluff trailing edge it will be seen that the lift-curve slope away from $\bar{\alpha}$ is slightly higher when the bevel is on the suction surface, than when the suction surface is completely flat. This effect, no doubt, arises from the fact that the bevel is equivalent to a small leading edge camber. The mean of the results for the two surfaces is shown dotted and this dotted curve is taken as the lift-curve slope for an infinitely thin wing. This same dotted curve is shown also on the lower graph of Fig. 5 and on the results for all the cambered wings. The results for the sharp trailing edge again show that the bevel on the upper surface produces slightly more lift than the flat surface, but that the sharp trailing edge appears to reduce the lift-curve slope slightly relative to that of the bluff trailing edge.

3.2 Cambered wing results

The variations of C_L with α and of $\Delta C_L / \Delta \alpha$ with $(\alpha - \bar{\alpha})$ for all the cambered wings are presented in Figs. 6 and 7 while summaries of the surface oil-flow patterns and vortex positions are given in Figs. 8 and 9. The attachment and secondary separation lines plotted in Fig. 8 were measured at about 80% chord. The attachment line is the line where the main flow over the vortex attaches to the wing. The secondary separation is the separation which occurs out-board of the vortex as the cross-flow from the attachment line passes through the suction peak and flows into an adverse gradient near the leading

edge. It will be seen from Fig. 7 that the curves of $\Delta C_L/\Delta\alpha$ against $(\alpha - \bar{\alpha})$ for wings 5, 6 and 7 do not have a clearly defined apex so that a value of $\bar{\alpha}$ could not be determined directly from Fig. 7. However, when these curves were studied in conjunction with the surface oil flows it was found that there was an incidence range in which the flow appeared to be attached on both surfaces. The centre of this incidence range has been taken as $\bar{\alpha}$. On the other hand for wings** 2 and 3 there was only a very small incidence range (about $\frac{1}{2}°$) in which the oil flow showed that the flow was attached to the wing on both surfaces; this incidence range corresponds closely to the apex of the curves of $\Delta C_L/\Delta\alpha$ against α. The vertical lines on Fig. 6 correspond to $\bar{\alpha}$ and the dotted lines show the corresponding lift which would be developed by the flat wing at the same incidence about attachment.

For wings 2 and 3 with $\beta = 0.15$ it can be seen that away from the attachment point both wings develop more lift than the flat wing, yet at the attachment point the lift-curve slope is identical with that of the flat wing. Furthermore the size of increase depends on the leading edge droop angle, being greater for wing 3 with a droop angle of 36.8° than for wing 2 where the droop angle is 16.7°. Below $\bar{\alpha}$ the lift-curve slope is less than that of the flat wing. The oil flow pictures showed that on the cambered wings there was a small incidence range about the attachment point where the flow near the edge formed a number of streamwise vortices, which coalesced into a single vortex as the incidence was increased. Once formed this vortex at first moved inboard less rapidly than the vortex on the flat wing but by $(\alpha - \bar{\alpha}) = 16°$ the vortices on both cambered wings were at approximately the same spanwise position as those on the flat wing. (Figs. 8 and 9). However, relative to the plane of the leading edge the vortices were higher on the cambered wings, the height above the edge increasing with leading edge droop. As noted in the last section it was impossible to get accurate measurements of vortex height when the vortex lay below the centre line. However, the results at higher incidence do suggest that the vortex initially rises much more rapidly on the cambered wings.

For wing 4, the wing with straight anhedral and $\beta = 0.3$, the surface oil-flow patterns were not clear. The smoke tests showed that the vortex was below the centre line until about $\alpha - \bar{\alpha} = 16°$, i.e. at $\alpha - \bar{\alpha} = 16°$ it was at approximately the same height above the leading edge as the vortex above wing 2, which has the same droop angle. For this wing the $\Delta C_L/\Delta\alpha$ curves have a clear apex and it can be seen that the lift-curve slope at $\alpha = \bar{\alpha}$ is higher than that of the flat wing, also that the increase in $\Delta C_L/\Delta\alpha$ with $(\alpha - \bar{\alpha})$ is greater.

** No clear oil flow results could be obtained for wing 4.

When we come to wing 5 there is a change of character in the curves of $\Delta C_L/\Delta\alpha$ against $(\alpha - \bar{\alpha})$, (Fig. 7). Instead of giving a clear apex the curve is relatively flat near $\alpha = \bar{\alpha}$ and then starts to increase rapidly at higher values of $(\alpha - \bar{\alpha})$; once this increase has started the lift-curve slope becomes much greater than that of the flat wing. This behaviour is associated with the fact that on this wing the flow appeared to be attached at the leading edge for a fair incidence range before first forming streamwise vortices and then a single vortex. Once this vortex had formed it moved inboard rapidly, (Fig. 8). Fig. 9 shows that the vortex positions at given $(\alpha - \bar{\alpha})$ are slightly further from the wing than on wing 3, and are certainly much higher than on wing 4 where the vortex is just level with the centre line at $(\alpha - \bar{\alpha}) = 16°$. This effect is also shown in the comparisons with the theoretical predictions presented in Fig. 16.

The change in character noted for wing 5 becomes more pronounced on wings 6 and 7 and in fact wing 7 shows a distinct jump in lift at $(\alpha - \bar{\alpha}) = 10°$. The surface oil patterns for this wing showed that the flow development near the leading edge was similar to that on wing 5, but that in addition a second vortex formed just inboard of the shoulder (see sketch in Fig. 9). The two vortices increased in size until at $(\alpha - \bar{\alpha}) = 10$ they suddenly combined to form a single vortex and so gave a jump in lift. The surface flow patterns were less clear on wing 6. Certainly there was no vortex inboard of the shoulder, on the other hand the oil motion in this region was sluggish, suggesting a thick boundary layer. The main attachment line moved in rapidly between $(\alpha - \bar{\alpha}) = 8°$ and $12°$. An attempt was made to suppress the inboard vortex on wing 7 with transition wires outboard of the shoulder, but without success. However, it is felt that these results may be sensitive to variations in Reynolds number and so less attention should be paid to these two wings.

In order to put the lift results into perspective the curves of $\Delta C_L/\Delta\alpha$ against $(\alpha - \bar{\alpha})$ for wings 1 to 5 are replotted on the same origin in Fig. 10. The upper figure shows the results as taken directly from Fig. 7, while in the lower figure C_L is based on developed area rather than projected area. From the top figure it can be seen that above $(\alpha - \bar{\alpha}) = 4°$ the lift-curve slopes of wings 2 and 4 are almost the same and that above $(\alpha - \bar{\alpha}) = 10°$, the slopes of wings 3 and 5 are the same. However, at incidences near $\bar{\alpha}$ there are differences caused by the initial type of development on wing 5, and the different minimum slopes at $\alpha = \bar{\alpha}$. When compared on a developed area basis this last effect is almost eliminated, and at higher incidences the lift-curve slopes of wings 4 and 5 are slightly lower than the slopes of wings 2 and 3 respectively. From these comparisons it

would appear that at incidences where the vortex flow is established the main factor determining the non-linear lift is the leading edge droop angle, rather than the total droop. This conclusion is also in line with the observations for vortex position, which again show that the position is mainly determined by leading edge droop angle.

The variations of C_m with C_L and of C_D with C_L^2 for all the wings are presented in Figs. 11 and 12. Again a vertical line has been drawn on the curves of C_m against C_L to indicate the attached point, while the dotted line shows the corresponding pitching moment curve of the flat wing about the attachment point. In general the effects of camber on pitching moment are small showing that distribution of vortex lift along the wing is not greatly affected by droop. Again it should be noted that the sudden changes in pitching moment for wings 6 and 7 may be affected by Reynolds number.

The drag results are best understood by noting that on wings 1 and 4 (the flat wing and the wing with anhedral) the main effect of the non-linear lift is to reduce the incidence for a given lift and so to reduce $\frac{\partial C_D}{\partial C_L^2}$ as lift, or incidence, is increased. On the other hand for the curved cambered wings there is an additional effect since the vortex produces low pressure on forward facing surfaces and so further reduces drag. This latter effect is considerably modified by the addition of thickness.

4. Theoretical Investigation

4.1 Mathematical Model

In the past a number of mathematical models have been proposed to deal with the presence of the leading edge vortex. Of these models the simplest one which gives the vortex strength and position in addition to the non-linear lift is that due to Brown and Michael[6]. From comparisons with experiment it has been found that this mathematical model gives reasonable agreement with the measured non-linear lift and measured vertical position of the vortex. However, the vortex core is always much nearer the wing centre line than the theory predicts. In this mathematical model Brown and Michael replaced the rolled up vortex sheet by a concentrated vortex core joined to the leading edge by a feeding sheet of vorticity (Fig. 13). Instead of making the core and the feeding sheet lie along streamlines as in the real fluid they postulated that the total force on the vortex system must be zero. By using this condition, and the condition that the flow leaves the leading edge smoothly they were able to obtain a solution within the framework of slender-body theory.

In conjunction with the present experimental programme the Brown and Michael model has been extended to cambered wings with

circular-arc cross-sections. This extension follows closely the work of Brown and Michael and uses the slender-body solution obtained by Smith[7] for the cambered wing without vortices. Details of the calculations are given in the Appendix and the results are plotted in Figs. 14 and 15. From these figures it can be seen that as the wing camber is increased the vortex core moves upwards and outwards relative to the vortex position on the flat wing. Also there is a slight increase in vortex strength at given incidence above the attachment incidence. (In the theory the attachment angle corresponds to the case of zero leading edge singularity in the absence of vortices). Fig. 15 shows that the non-linear lift also increases with camber. The relevance of these results to the present investigation is discussed in the next section.

It should be noted that there are two other mathematical models which give better agreement with experiments for flat wings than the Brown and Michael model. Pershing[8] suggests that the reason why the Brown and Michael model fails to predict the lateral position of the vortex is that they ignore the secondary separation which occurs on the wing surface outboard of the main vortex. Thus he suggests that the condition that the flow leaves the edge smoothly is unrealistic, and instead he fixes the vortex core height as $\alpha/4$ (or $(\alpha - \bar{\alpha})/4$ for cambered wings). Using this condition and Legendre's[9] condition that the vortex core lies on a streamline he obtains a solution which is in very good agreement with experiment, including the prediction of vortex position. (Pershing was unable to get a solution if he used the condition of zero force on the vortex system). This model was not used in the present investigation since an essential feature of the experimental results is that the vortex core height changes with camber. Mangler and Smith[10] have introduced a much more realistic model of the vortex sheet structure, and the necessary numerical analysis has been further developed and improved by Smith to give close agreement with measured results. In theory this model could be extended to cambered wings. However, because of the large amount of numerical work this has not been attempted.

4.2 Comparison with experiment

In Figs. 16 and 17 the theoretical results are compared with the experimental results; the results are compared at equal leading edge droop angles since this appears to be the main parameter to determine the experimental behaviour. In Fig. 16 the height of the vortex core above the leading edge for the various cambered wings is compared with the calculated height for circular arc sections with the same droop angle. The theoretical results are shown by lines; the line for $\phi = 40°$ is dotted as it was extrapolated from the results for $\phi = 17°$ and $\phi = 35.5°$ ($\beta = 0.15$ and 0.30), and is probably near the limit of the theory. At small droop angles the theoretical and experimental heights are in close agreement, but at higher droop angles the increase in height is underestimated by the theory. As pointed out in

section 4.1, the Brown and Michael model also shows the vortex core nearer the leading edge than it occurs in experiments, so no direct comparisons of the lateral positions of the vortex cores are presented. However, the calculated vortex paths of Fig. 14(a) show that at constant $(\alpha - \bar{\alpha})$ the effect of camber is to move the vortex core up, and out, relative to the leading edge; a similar movement is just discernible in the experimental results of Fig. 9. So the experimental and theoretical results for vortex position are in qualitative agreement when compared at equal leading edge droop angles.

There is a difficulty in comparing the lift measurements with the theory in that the theory is based on slender-body theory and so gives no loss of lift near the trailing edge. This effect is illustrated in Fig. 17(a) where the flat wing results are compared with theory. It will be seen that the measured lift is much lower than the theory predicts. At zero incidence the initial lift-curve slope of the flat wing is approximately 20% lower than theoretical slope of $\frac{\pi A}{2}$; at higher incidence the measured lift is much more than 20% lower than the theory. This discrepancy is caused, in part, by the simplifications introduced into the mathematical model. However, the moment curves of Fig. 11 have a tendency to 'pitch up' at higher incidence showing that the lift moves forward, i.e. the trailing edge effect becomes greater away from zero incidence. In view of these discrepancies a direct comparison of the measured lift of the cambered wings with the theoretical curves of Fig. 15 would be misleading. Instead in Fig. 17(b) the measured lift on wings 2, 3, 4 and 5 is compared with 'theoretical curves' for the appropriate ϕ given by

$$C_L = (C_L)_{\text{theory}} \times \left(\frac{(C_L)_{\text{measured}}}{(C_L)_{\text{theory}}} \right)_{\text{flat wing}} ,$$

i.e. it is assumed that trailing edge effects, and errors in the mathematical model, are independent of camber. For wings 2 and 4 ($\phi \approx 16.7°$) the 'theoretical' curve so obtained is in excellent agreement with the measured results, but for wing 3, the lift is lower than the theory. It is even lower on wing 5, but this is caused by the change in behaviour of the vortex development near $\alpha \approx \bar{\alpha}$.

Although the mathematical model shows quantitative discrepancies from experimental results, the qualitative effects of camber are shown. Thus it appears reasonable to assume that the mathematical model incorporates the significant features of the cambered shape, and so it may be used to discuss the mechanism which gives more non-linear lift.

5. Discussion of the Mechanism of Increased Non-linear Lift

In the discussion of the experimental results it has been shown that the main parameter which determines the effects of leading edge droop on the vortex development is the leading edge droop angle (ϕ). These tests do not give any indication of the mechanism which produces the increase in non-linear lift with leading edge droop, and it was mainly to explain this increase that the theoretical investigation of section 4 was undertaken.

The comparison of the theoretical results with the experimental results has shown that the simple mathematical model of Brown and Michael is capable of predicting the main effects of camber. From the theoretical results it can be seen that the main effects of camber are to increase the height of the vortex core above the leading edge and to increase the vortex strength. The percentage increase in height is somewhat greater than the increase in strength. However, when the change in wing shape is taken into account it is found that the percentage increase in normal distance from the wing surface is about the same as the percentage increase in vortex strength. Thus on a simple argument one might expect the cross-flow velocity at the wing surface due to the vortex to be virtually unchanged, and hence that there would be little change in pressure distribution, or lift. However, examination of the formula for cross-flow due to the vortex (eqn. (14) of the Appendix) shows that the velocity at the wing surface depends mainly on the position of the vortex in the transformed θ plane (see Fig. 13). The velocity increases as the vortex moves nearer the wing surface in this transformed plane. (This might be expected since in this plane the wing and the two vortices transform into a vertical plate with the vortices forming images of each other in it.) Fig. 18 shows the calculated vortex positions in this plane and it can be seen that as camber is increased the vortices move closer to the transformed wing surface. Typical values of the resulting cross-flow velocities due to the vortices on the actual wing surface are shown in Fig. 19 for $\frac{\alpha - \bar{\alpha}}{\epsilon} = 1.0$ and $\beta = 0$ and 0.3. This figure also includes the cross-flow velocity on the wings in the absence of the vortices at the same value of $(\alpha - \bar{\alpha})/\epsilon$. It can be seen that camber results in large increases in the cross-flow velocity and so gives much lower pressures on the upper surface. It is interesting to note that this increase in velocity occurs over most of the wing surface in spite of the fact that the singularity in the cross-flow velocity at the leading edge is reduced by camber. (This singularity is, of course, cancelled by the corresponding singularity which would exist in the cross-flow in the absence of the vortex).

The fact that in the transformed plane the vortices are nearer the wing surface for the cambered wings than for the plane wing, whereas the converse is true in the physical plane, suggests that the wing camber produces a large distortion of the flow field around the vortices. Thus it would appear that it is this distortion of the velocity field of the vortex, together with the

slight increase in vortex strength which accounts for the increase in non-linear lift. It should be noted that this distortion is associated with the shape of the wing surface and so would still occur in any investigations using more accurate representation of the vortex system.

6. Conclusions

Measurements have been made of the overall forces and vortex position on a series of delta wings with various types of leading edge droop. In addition a theoretical study of conically-cambered wings has been made using the Brown and Michael model. This theoretical investigation was undertaken in order to understand the mechanism of the non-linear lift development on cambered wings.

The results of the experimental programme may be summarised as follows.

(a) For leading edge droop angles less than about 40° the non-linear lift development is qualitatively similar to that on a flat wing, but the non-linear lift increases with droop angle and the vortex core height above the leading edge also increases.

(b) The increase in lift due to droop is appreciable; for example at 10° above the attachment incidence the lift is approximately 10% greater for a droop angle of 17° than on a flat wing at corresponding incidence.

(c) For droop angles greater than 40° the initial development of the leading edge vortex is greatly weakened, but at sufficiently high incidence the lift-curve slope becomes greater than on wings with smaller droop angles.

A comparison of the theoretical and experimental results shows that the mathematical model predicts qualitatively the main camber effects. From the mathematical model it can be deduced that the increase in non-linear lift on the cambered wings is caused by a slight increase in vortex strength, together with a large distortion of the velocity field around the vortex. This distortion causes higher cross-flow velocities on the wing upper surface and hence lower pressures.

References

1. Maskell, E.C.
   Weber, J.
   On the aerodynamic design of slender wings.
   J. Roy. Aero. Soc. Vol. 63, pp.709-721, 1959.

2. Squire, L.C.
   Further experimental investigations of the characteristics of cambered gothic wings at Mach numbers from 0.4 to 2.0.
   A.R.C. R & M 3310, 1961.

3. Keating, R.F.A.
   Low-speed wind-tunnel tests on sharp-edged gothic wings of aspect ratio 3/4.
   A.R.C. C.P. 576, 1960.

4. Squire, L.C.
   The characteristics of some slender cambered gothic wings at Mach numbers from 0.4 to 2.0.
   A.R.C. R & M 3370, 1962.

5. Peckham, D.
   Atkinson, S.A.
   Preliminary results of low-speed wind-tunnel tests on a gothic wing of aspect ratio 1.0.
   A.R.C. C.P. 508, 1957.

6. Brown, C.E.
   Michael, W.H.
   On slender delta wings with leading-edge separation.
   N.A.C.A. T.N. 3430, 1955.

7. Smith, J.H.B.
   The properties of a thin conically cambered wing according to slender-body theory.
   A.R.C. R & M 3135, 1958.

8. Pershing, B.
   Separated flow past slender delta wings with secondary vortex simulation.
   Aerospace Corporation,
   SSD-TDR-64-151/TD269-4560-10-4,
   (AD 607 442), 1964.

9. Legendre, R.
   Ecoulement au voisinage de la pointe avant d'une aile à forte flèche aux incidences moyennes.
   La Recherche Aèronautique No. 30, pp.3-8, 1952; and No. 31, pp.3-6, 1953.

10. Mangler, K.W.
    Smith, J.H.B.
    A theory of the flow past a slender delta wing with leading edge separation.
    Proc. Roy. Soc. A. Vol. 251, pp.200-217, 1959.

Appendix

Details of Calculation of Vortex Positions and Strengths

As discussed in section 4, Brown and Michael replace the rolled up vortex sheet by a concentrated vortex core joined to the leading edge by a plane feeding sheet of vorticity. They then used slender-body theory and solved the problem in the cross-flow plane with the following boundary conditions:

(i) Zero velocity normal to the wing surface.

(ii) The flow leaves the leading edge smoothly.

(iii) Zero total force on the vortex and the feeding sheet.

The notation for the present investigation, together with the conformal transformations used to find the complex potential in the cross-flow plane, is illustrated in Fig. 13. It should be noted that for the uncambered wing considered by Brown and Michael the Z-plane is identical to the σ-plane. In the Z-plane the last boundary condition is

$$(v + iw)_{1,Z=Z_o} = V\epsilon\left(\frac{2Z_o}{a} - 1\right)$$

$$\text{or} \qquad (v - iw)_{1,Z=Z_o} = V\epsilon\left(\frac{2\bar{Z}_o}{a} - 1\right) \tag{1}$$

where $(v + iw)_{1,Z=Z_o}$ represents the average velocity at the position of the right-hand vortex and is found by subtracting the velocity field of the vortex at Z_o from the total velocity and taking the limit as $Z \to Z_o$.

For the flat wing with $\sigma \equiv Z$ Brown and Michael found the complex potential by the transformation $\theta^2 = \sigma^2 - a^2$ giving, in the σ-plane,

$$W(\sigma) \equiv W(Z) = -\frac{i\Gamma}{2\pi} \log \frac{\sqrt{\sigma^2 - a^2} - \sqrt{\sigma_o^2 - a^2}}{\sqrt{\sigma^2 - a^2} + \sqrt{\bar{\sigma}_o^2 - a^2}} - iV\alpha\sqrt{\sigma^2 - a^2}\,, \tag{2}$$

where the first term is the potential of the concentrated vortices and the second is that of the free stream at incidence α. The transformation $\theta^2 = \sigma^2 - a^2$ is singular at the wing leading edges so that in order to satisfy the second boundary condition we must have

$$\frac{dW}{d\theta} = 0, \quad \text{at} \quad \theta = 0,$$

$$\text{or} \quad \frac{2\pi V\alpha}{\Gamma} = \frac{1}{\sqrt{\sigma_o^2 - a^2}} + \frac{1}{\sqrt{\bar{\sigma}_o^2 - a^2}} \, . \tag{3}$$

Eqn. (1) may be written

$$\left\{ \frac{dW(\sigma)}{d\sigma} + \frac{i\Gamma}{2\pi} \frac{1}{\sigma - \sigma_o} \right\}_{\sigma \to \sigma_o} = V\epsilon \left(\frac{2\sigma_o}{a} - 1 \right) . \tag{4}$$

When α is eliminated from eqn. (2) by use of eqn. (3) and the resulting expression for $W(\sigma)$ substituted into eqn. (4) an equation for σ_o is obtained in terms of the parameter $\Gamma/V\epsilon$. This equation can be solved for the physical positions of the vortices by separation of the equation into its real and imaginary parts and then finding values of y_o/a and z_o/a (the ordinates of the vortex position) which give the same value of $\Gamma/V\epsilon$ in the two equations.

For the case of the wing with conical camber in the form of a circular arc we use the transformation

$$\frac{\sigma}{a} = \frac{Z - i\beta a}{a - i\beta Z}$$

to transform the circular arc in the Z-plane to the flat plate in the σ-plane. This transformation, which was introduced by Smith[7], transforms the point at infinity in the Z-plane to the finite point, $\sigma = \frac{ia}{\beta}$, in the σ-plane. The positions of the vortices are only changed slightly by this transformation.

In the σ-plane Smith shows that the complex potential corresponding to a uniform flow at incidence α is

$$W(\sigma) = \frac{V\epsilon a \cos\alpha (1 + \beta^2)^2}{4\beta^2} \log \frac{(a - i\beta\sigma)(a\sqrt{1 + \beta^2} + i\beta\sqrt{\sigma^2 - a^2})}{(a + i\beta\sigma)(a\sqrt{1 + \beta^2} - i\beta\sqrt{\sigma^2 - a^2})}$$

$$+ \frac{iV\epsilon a^2 \cos\alpha (1 - \beta^2)\sqrt{1 + \beta^2}}{2\beta(\sigma\sqrt{1 + \beta^2} + \sqrt{\sigma^2 - a^2})} - \frac{iVa^2 \sin\alpha \sqrt{1 + \beta^2}}{\beta(\beta\sqrt{\sigma^2 - a^2} - ia\sqrt{1 + \beta^2})} \tag{5}$$

To this complex potential must be added the potential for the vortices at σ_o and $-\bar{\sigma}_o$, i.e.

$$W(\sigma) = -\frac{i\Gamma}{2\pi}\log\frac{\sqrt{\sigma^2 - a^2} - \sqrt{\sigma_o^2 - a^2}}{\sqrt{\sigma^2 - a^2} + \sqrt{\bar{\sigma}_o^2 - a^2}} \quad . \tag{6}$$

Although this complex potential gives finite velocities at the point ia/β these velocities tend to zero in the Z-plane.

Eqn. (5) results in very complicated algebra and so is simplified by ignoring terms of $O(\beta^3)$ and putting $\cos\alpha = 1$, $\sin\alpha = \alpha$. The final equation for the complex potential in the σ-plane becomes

$$W(\sigma) = -\frac{iV\epsilon\, a}{6}\frac{\beta}{a^3}\left(\sigma - \sqrt{\sigma^2 - a^2}\right)\left(\sigma^2 - \sigma\sqrt{\sigma^2 - a^2} + 7a^2\right)$$

$$- iV\alpha\left[\sqrt{\sigma^2 - a^2} + \frac{i\beta}{2a}(a^2 - 2\sigma^2) + \frac{\beta^2}{2a^2}(a^2 - 2\sigma^2)\sqrt{\sigma^2 - a^2}\right]$$

$$- \frac{i\Gamma}{2\pi}\log\frac{\sqrt{\sigma^2 - a^2} - \sqrt{\sigma_o^2 - a^2}}{\sqrt{\sigma^2 - a^2} + \sqrt{\bar{\sigma}_o^2 - a^2}} \quad . \tag{7}$$

The condition that the flow leaves the edge smoothly is

$\frac{dW}{d\theta} = 0$ at $\theta = 0$, or $\frac{dW}{d\sigma} \times \frac{\sqrt{\sigma^2 - a^2}}{\sigma} = 0$ at $\sigma = a$, giving

$$\frac{\Gamma}{2\pi}\left[\frac{1}{\sqrt{\sigma_o^2 - a^2}} + \frac{1}{\sqrt{\bar{\sigma}_o^2 - a^2}}\right] = V\alpha\left(1 - \frac{\beta^2}{2}\right) - \frac{3}{2}V\epsilon\beta. \tag{8}$$

This last equation shows that $\Gamma = 0$ at

$$\frac{\alpha}{\epsilon} = \frac{3}{2}\beta\left(1 + \frac{\beta^2}{2}\right) . \tag{9}$$

As might be expected this is the angle found by Smith for zero leading edge singularity; it will be defined as $\bar{\alpha}$, the attachment angle.

The condition that the vortex system is force free (eqn. (1)) gives

$$V\epsilon\left(\frac{2\bar{Z}_o}{a} - 1\right) = \left(\frac{dW}{d\sigma} \cdot \frac{d\sigma}{dZ} + \frac{1}{2\pi}\frac{1}{Z - Z_o}\right)_{Z \to Z_o} . \qquad (10)$$

Elimination of α from eqn. (7) by means of eqn. (8) and then substitution into eqn. (10) gives, after some lengthy algebra,

$$\frac{2\pi V\epsilon}{\Gamma}\left[\left(\frac{2\bar{Z}_o}{a} - 1\right)\frac{(a - i\beta Z_o)^2}{a^2(1 + \beta^2)} + \frac{3}{2} i \frac{\beta}{a}\left(\frac{\sigma_o}{\sqrt{\sigma_o^2 - a^2}} - 2i\frac{\beta}{\alpha}\sigma_o\right)\right.$$

$$\left. + \frac{i\beta}{2a^2}\left((2\sigma_o^2 + 2a^2) - \frac{\sigma_o}{\sqrt{\sigma_o^2 - a^2}}(2\sigma_o^2 - a^2)\right)\right] =$$

$$\frac{i\sigma_o}{\sqrt{\sigma_o^2 - a^2}} \cdot \frac{1}{\sqrt{\sigma_o^2 - a^2} + \sqrt{\bar{\sigma}_o^2 - a^2}} + \frac{i}{2a}\frac{(a - i\beta Z_o)^3(1 - \beta^2)}{(Z_o - i\beta a)(Z_o^2 - a^2)}$$

$$+ \beta(a - i\beta Z_o)$$

$$- i\left(\frac{1}{\sqrt{\sigma_o^2 - a^2}} + \frac{1}{\sqrt{\bar{\sigma}_o^2 - a^2}}\right)\left(1 + \frac{\beta^2}{2}\right)\left(\frac{\sigma_o}{\sqrt{\sigma_o^2 - a^2}} - 2i\frac{\beta\sigma_o}{a}\right.$$

$$\left. + \frac{\beta^2}{2a^2}\sigma_o\frac{(5a^2 - 6\sigma_o^2)}{\sqrt{\sigma_o^2 - a^2}}\right) \qquad (11)$$

where Z_o and σ_o are the vortex positions in the Z-plane and σ-plane respectively. This complex equation was split into its real and imaginary parts and the resulting two equations solved by finding values of $\frac{y_o}{a}$ and $\frac{z_o}{a}$, the real and imaginary parts of Z_o, which gave equal values of $\frac{2\pi V\epsilon}{\Gamma}$; once these values were found eqn. (8) was used to find the corresponding value of α. The results are plotted in Fig. 14 for $\beta = 0$, 0.15 and 0.30.

The lift acting on the wing can be found by contour integration to give

$$L = -\rho U \Re\int_C W dZ, \quad \text{where the contour } C \text{ contains}$$

the wake. The contribution to this integral of the complex potential given in eqn. (5) has been evaluated by Smith, while that due to eqn. (6) can be found by finding the imaginary part of the coefficient of $1/Z$ in the expansion of $W(Z)$. Carrying through this expansion and adding the resulting lift to that obtained by Smith, we find that to $O(\beta^2)$ the lift coefficient is given by

$$\frac{C_L}{\epsilon^2} = 2\pi\left\{\frac{\alpha}{\epsilon}\left(1 + \frac{\beta^2}{2}\right) - \frac{5}{4}\beta\right\} + \frac{4\Gamma(1+\beta^2)^{\frac{1}{2}}y_2}{Va^2\epsilon\left[\left((1+\beta^2)^{\frac{1}{2}} - z_2\beta\right)^2 + \beta^2 y_2{}^2\right]} \tag{12}$$

where y_2 and z_2 are the real and imaginary parts of the vortex position in the Θ-plane, i.e. $\Theta_o = y_2 + iz_2$.

At $\alpha = \bar{\alpha}$ $\left(= \frac{3}{2}\beta(1 + \beta^2/2)\right)$

$$\frac{C_L}{2} = \frac{\pi\beta}{2} + O(\beta^3) ,$$

and we may rewrite eqn. (12) as

$$\frac{C_L - \bar{C}_L}{\epsilon^2} = 2\pi\left(\frac{\alpha - \bar{\alpha}}{\epsilon}\right)\left(1 + \beta^2/2\right) + \frac{4\Gamma(1+\beta^2)^{\frac{1}{2}}y_2}{Va^2\epsilon\left[\left((1+\beta^2)^{\frac{1}{2}} - z_2\beta\right)^2 + \beta^2 y_2{}^2\right]}. \tag{13}$$

Curves of $\left(\frac{C_L - \bar{C}_L}{\epsilon^2}\right)$ against $\left(\frac{\alpha - \bar{\alpha}}{\epsilon}\right)$ are plotted in Fig. 15.

The cross-flow velocity on the wing surface is given by

$q = \left|\frac{dW}{dZ}\right| = \left|\frac{dW}{d\sigma} \cdot \frac{d\sigma}{dZ}\right|$. Thus from eqn. (6) we obtain for the cross-flow due to the vortices

$$\frac{\sqrt{1 - \frac{y^2}{a^2}}}{V} q = - \frac{\Gamma}{2\pi a V \epsilon} \cdot \frac{(y/a)(1 - 2\beta^2 + \beta^2 y^2/_a 2) . 2(y_2/a)}{\left(\frac{y^2}{a}\right)^2 + \left(b - \frac{z_2}{a}\right)^2} \quad (14)$$

where y_2 and z_2 are the vortex positions in the Θ-plane, $\frac{y}{a}$ is the local spanwise position and $b = \pm \sqrt{1 - y^2/_a 2}\ (1 + \beta^2\ y^2/_a 2)$; the positive root corresponding to the wing upper surface and the negative root to the lower surface.

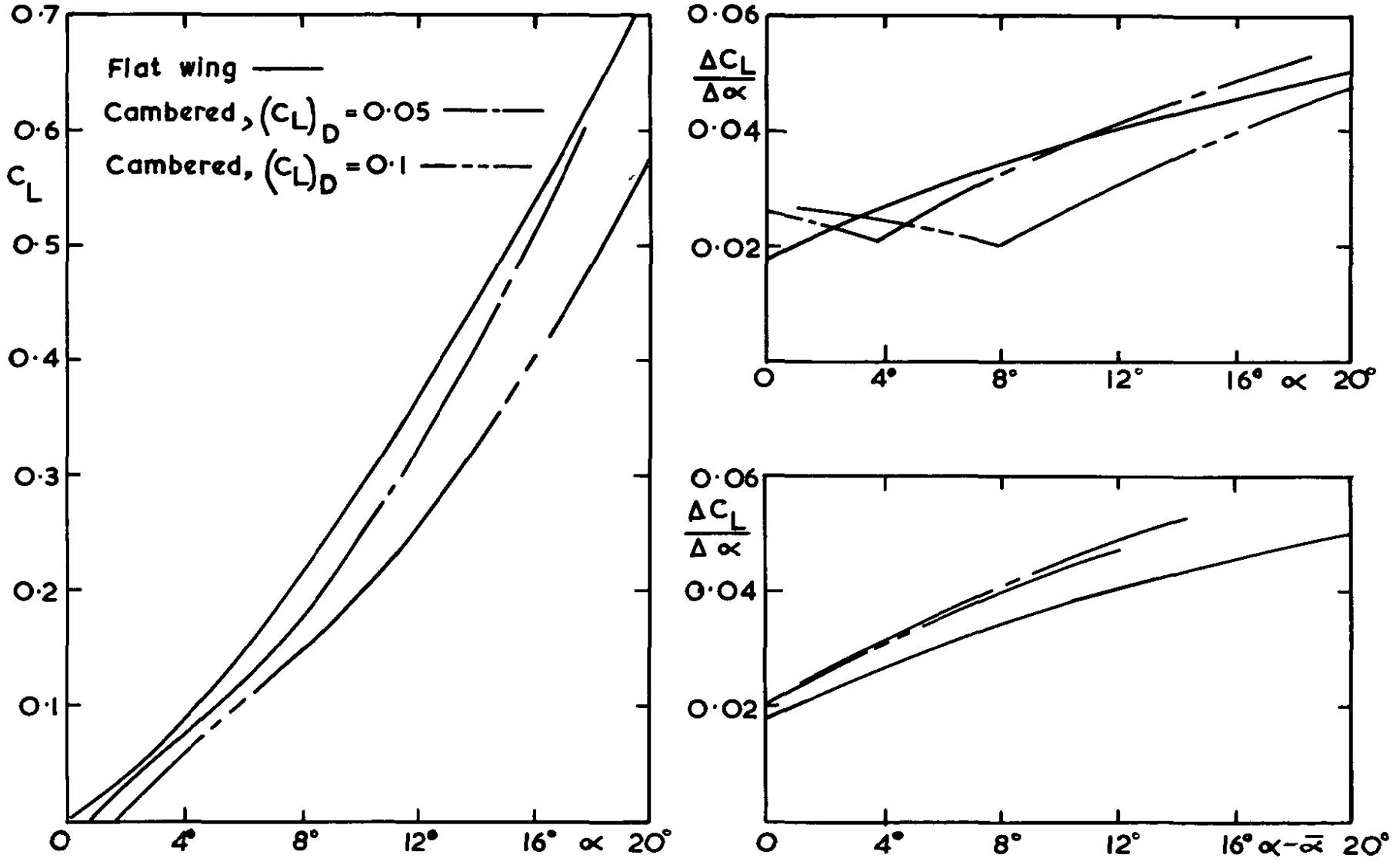

FIG. 1. LIFT RESULTS FOR WINGS OF REFS 2 AND 3

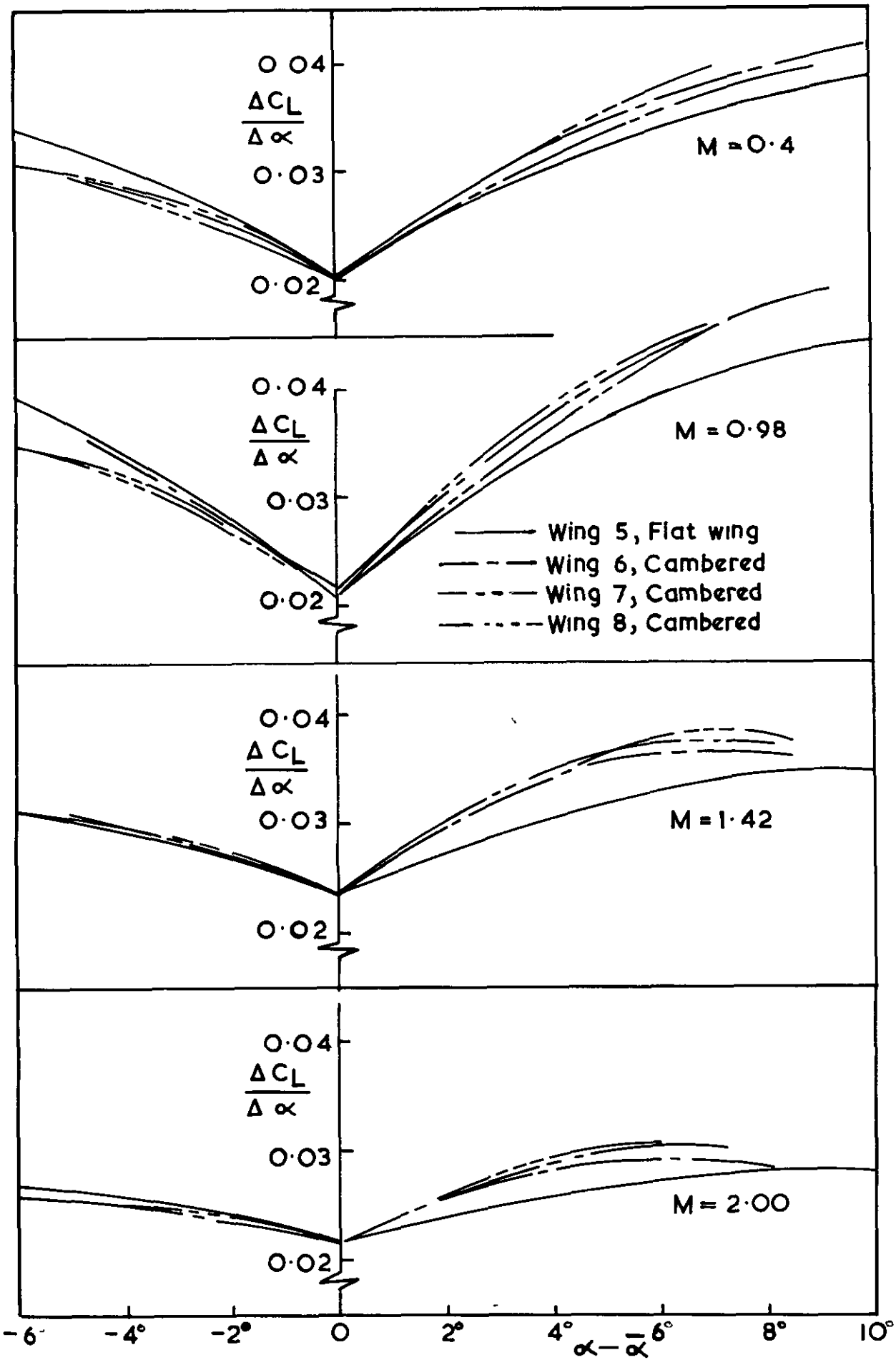

FIG. 2 NON – LINEAR LIFT OF WING OF REF 4.

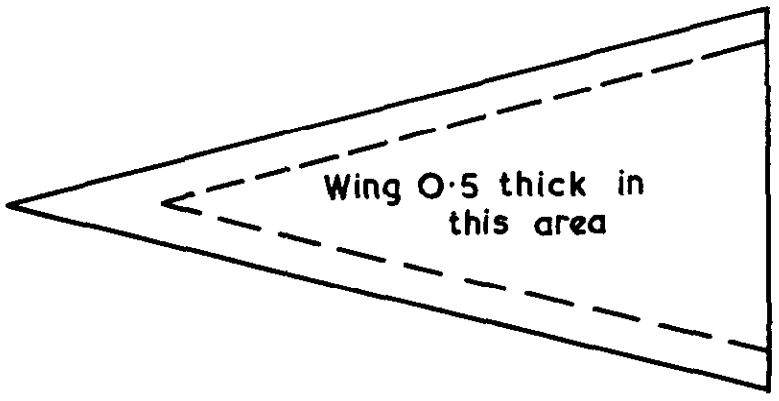

PLANFORM: ASPECT RATIO 1·0
ROOT CHORD 40"

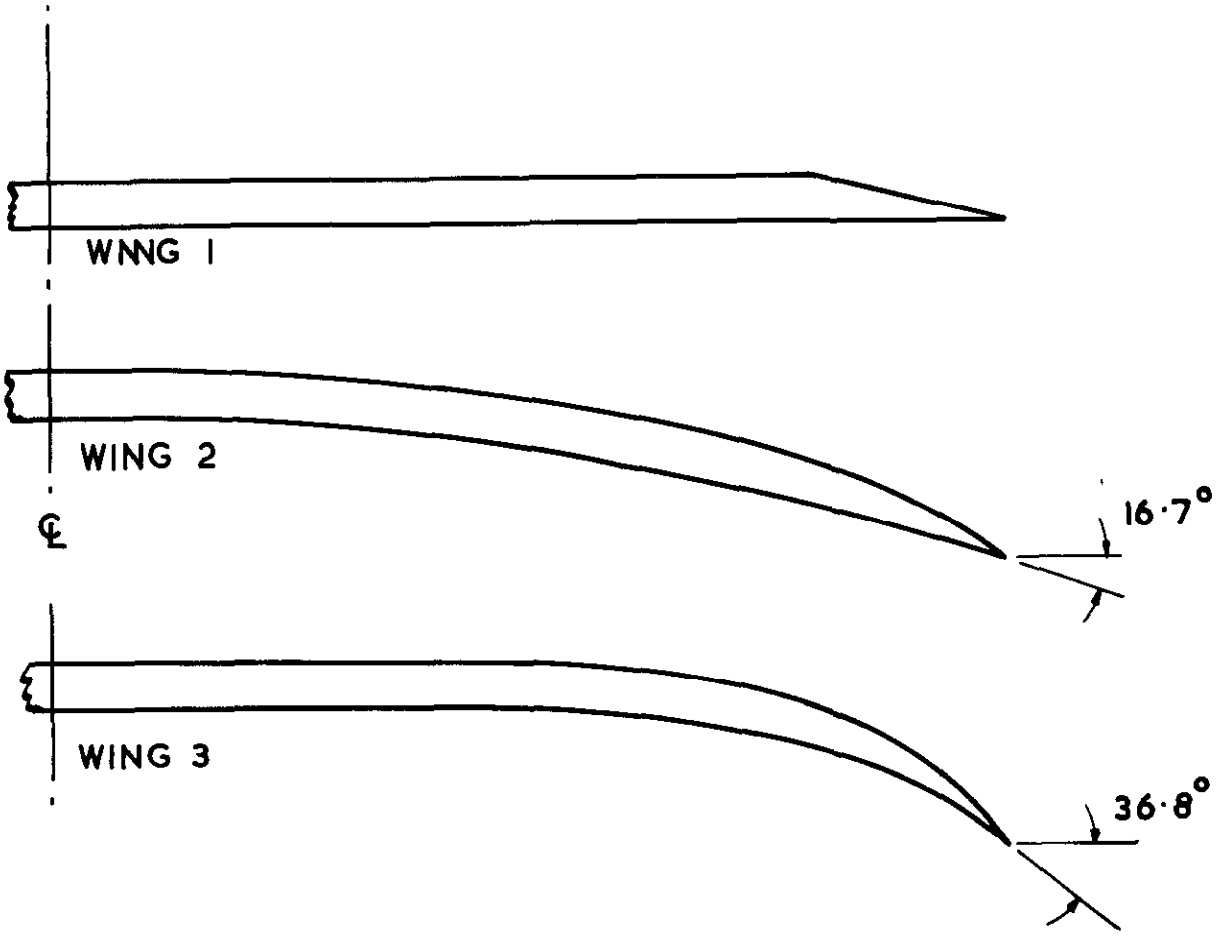

CROSS-SECTIONS AT TRAILING EDGE:
LOWER SURFACES CONICAL

FIG. 3 (a) DETAILS OF MODELS; FLAT WING AND $\beta = 0 \cdot 15$

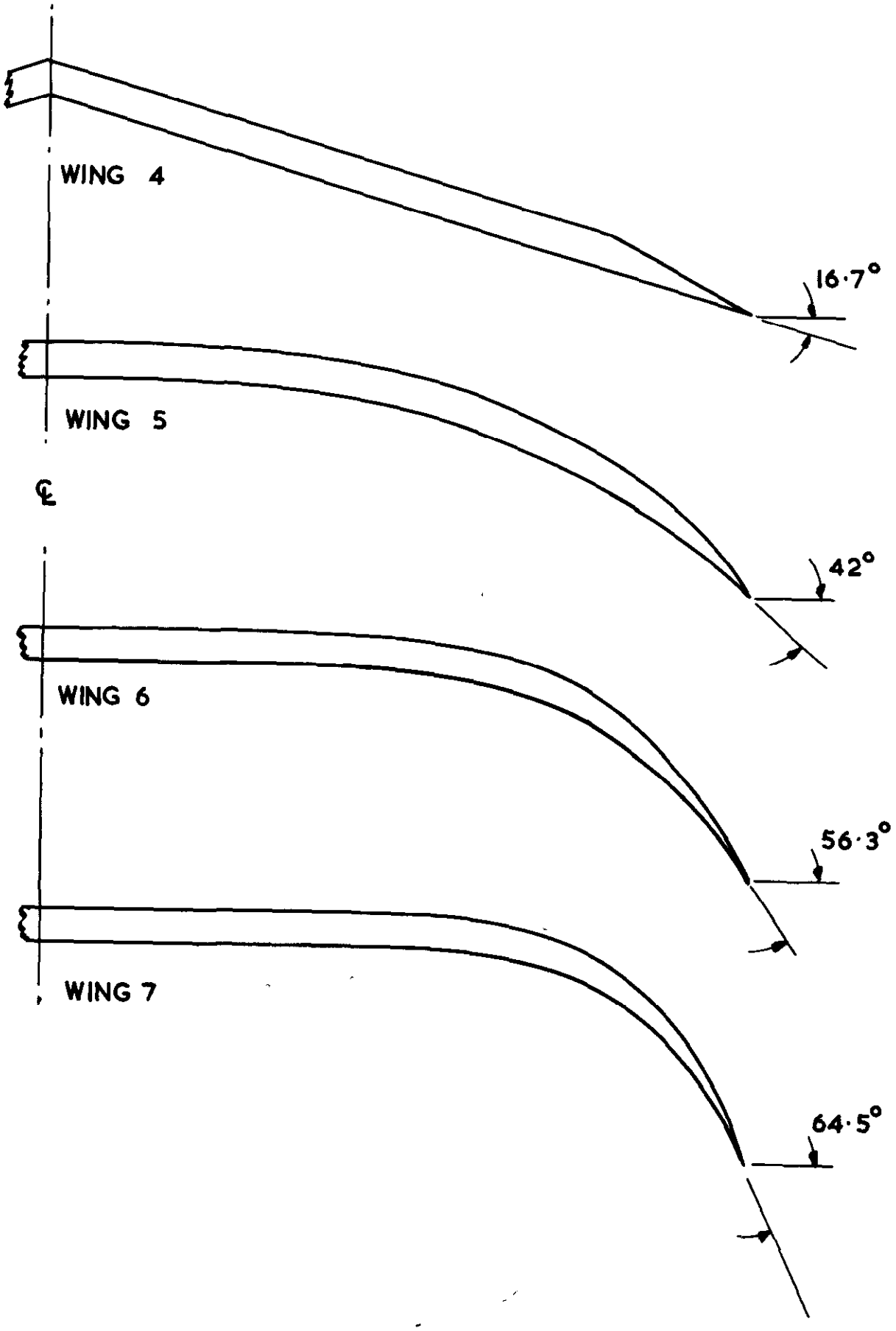

FIG. 3 (b) DETAILS OF MODELS : $\beta = 0 \cdot 3$

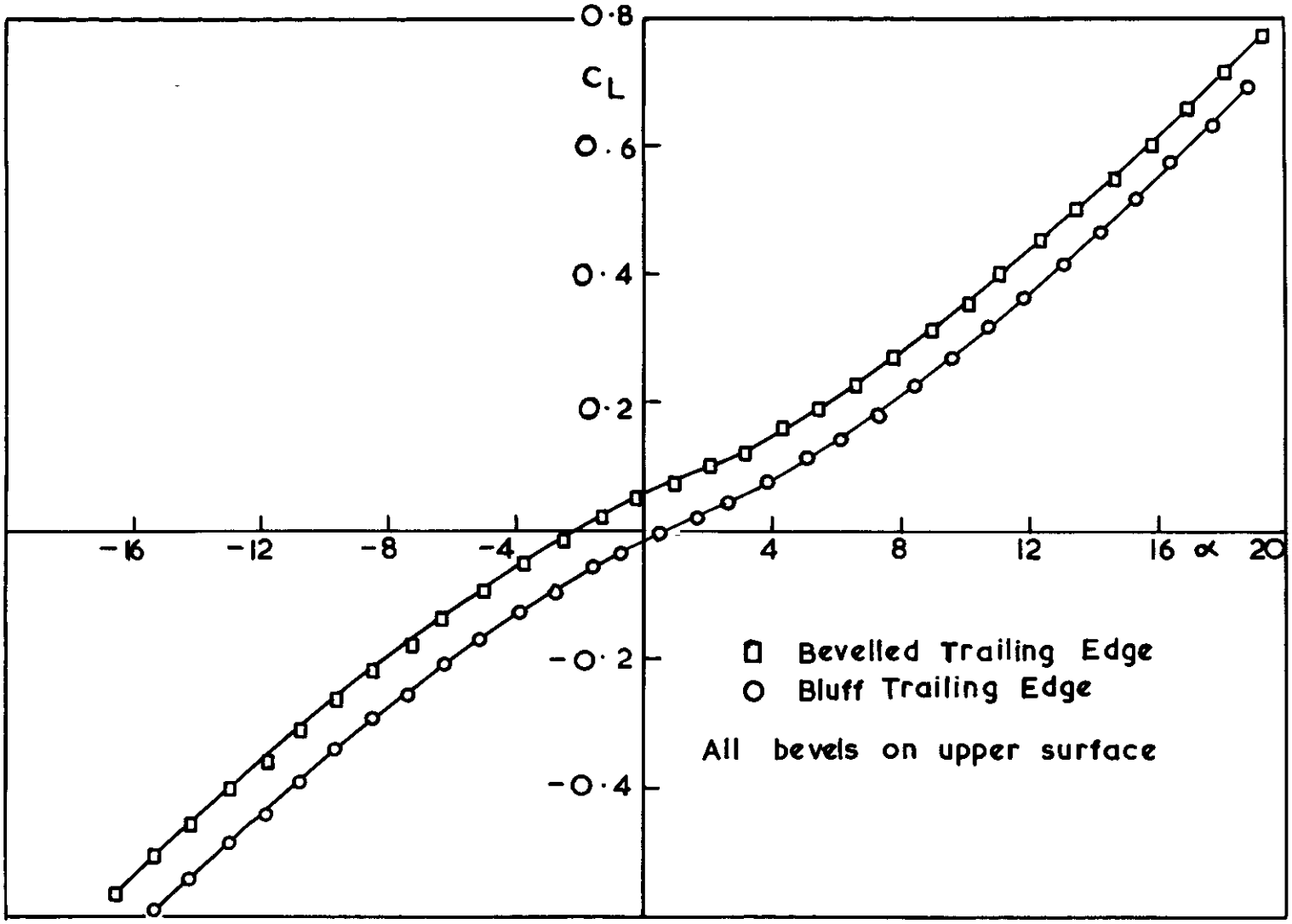

FIG. 4 C_L AGAINST ∝ FOR FLAT WINGS

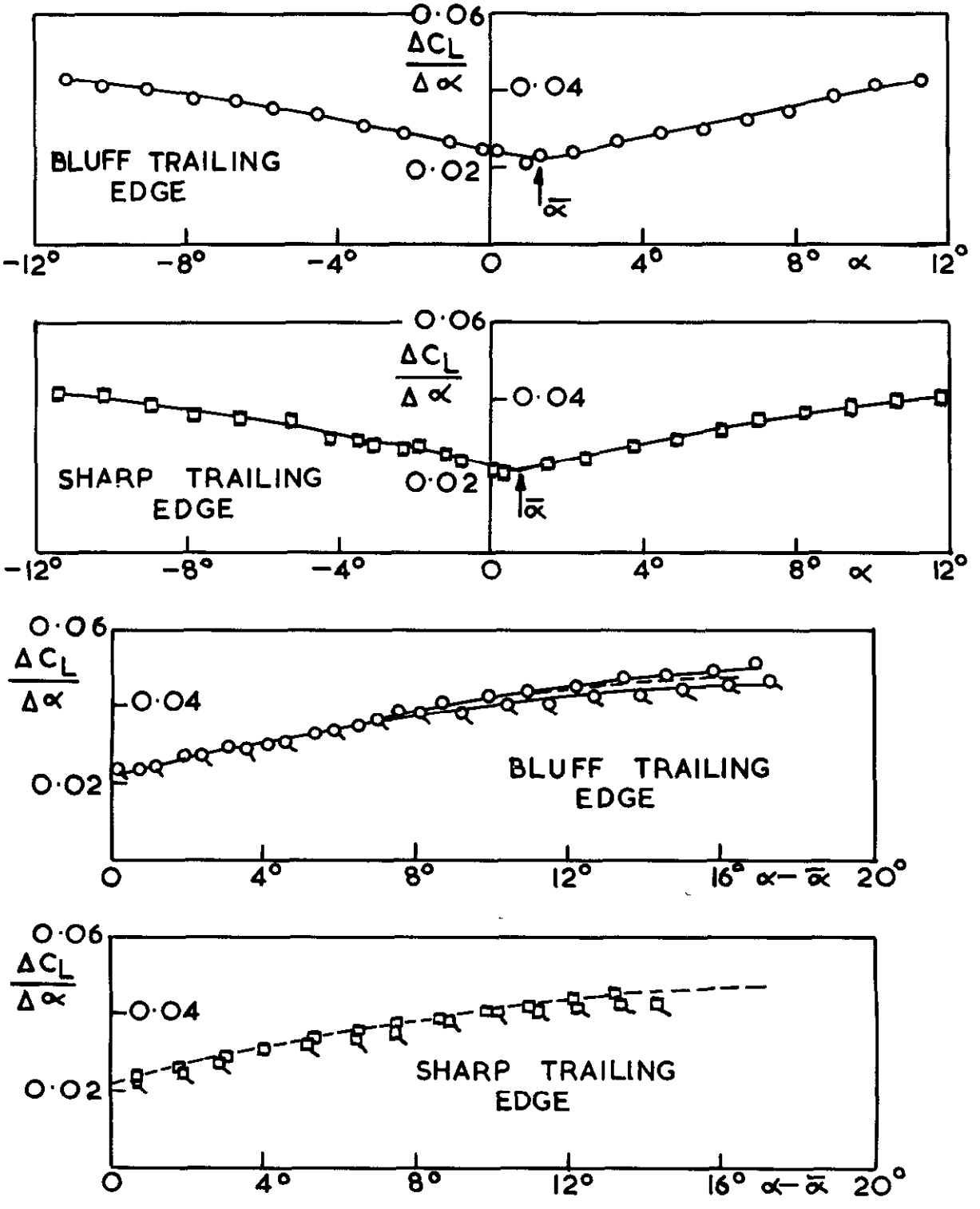

FIG 5 ANALYSIS OF FLAT WING LIFT

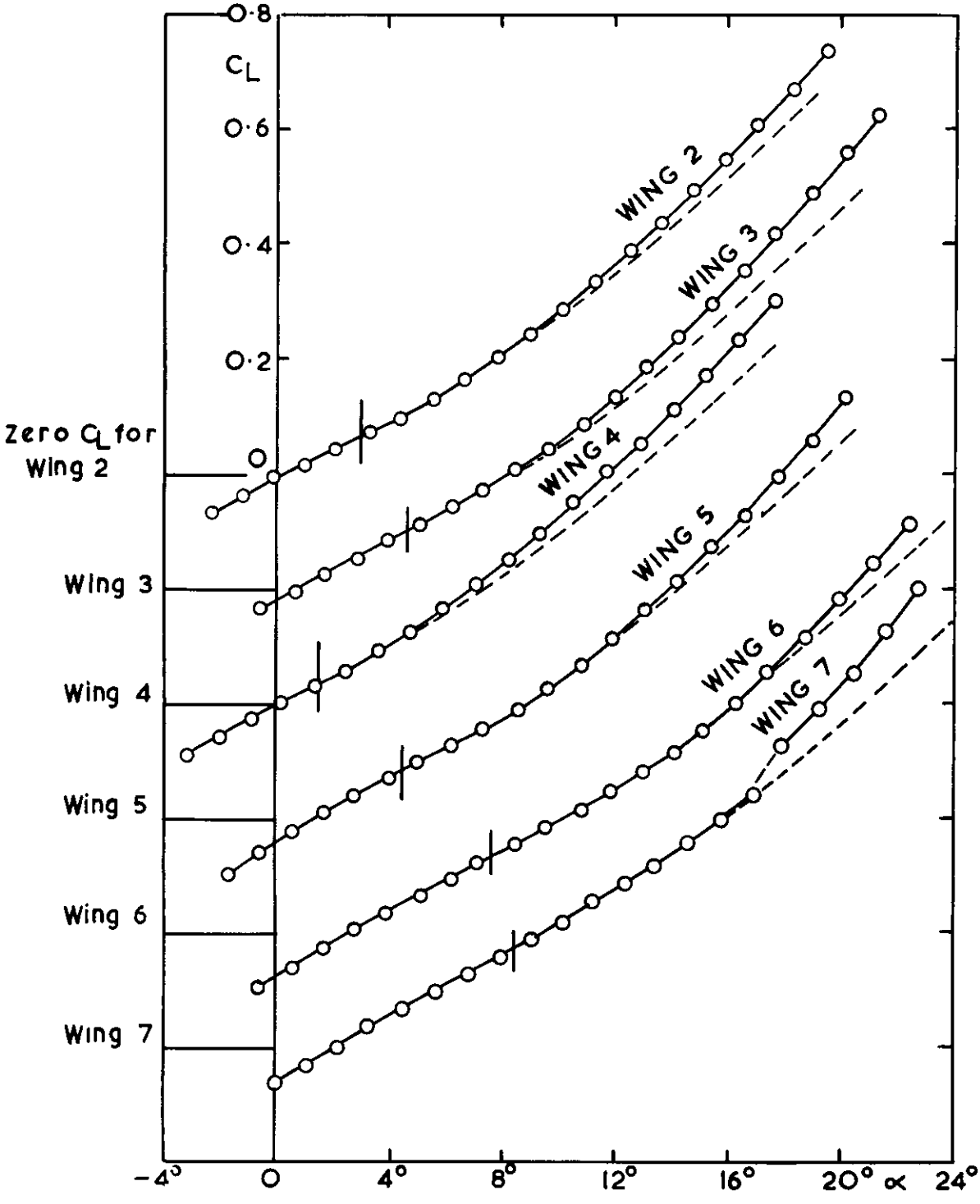

FIG 6 C_L AGAINST ∝ · CAMBERED WINGS

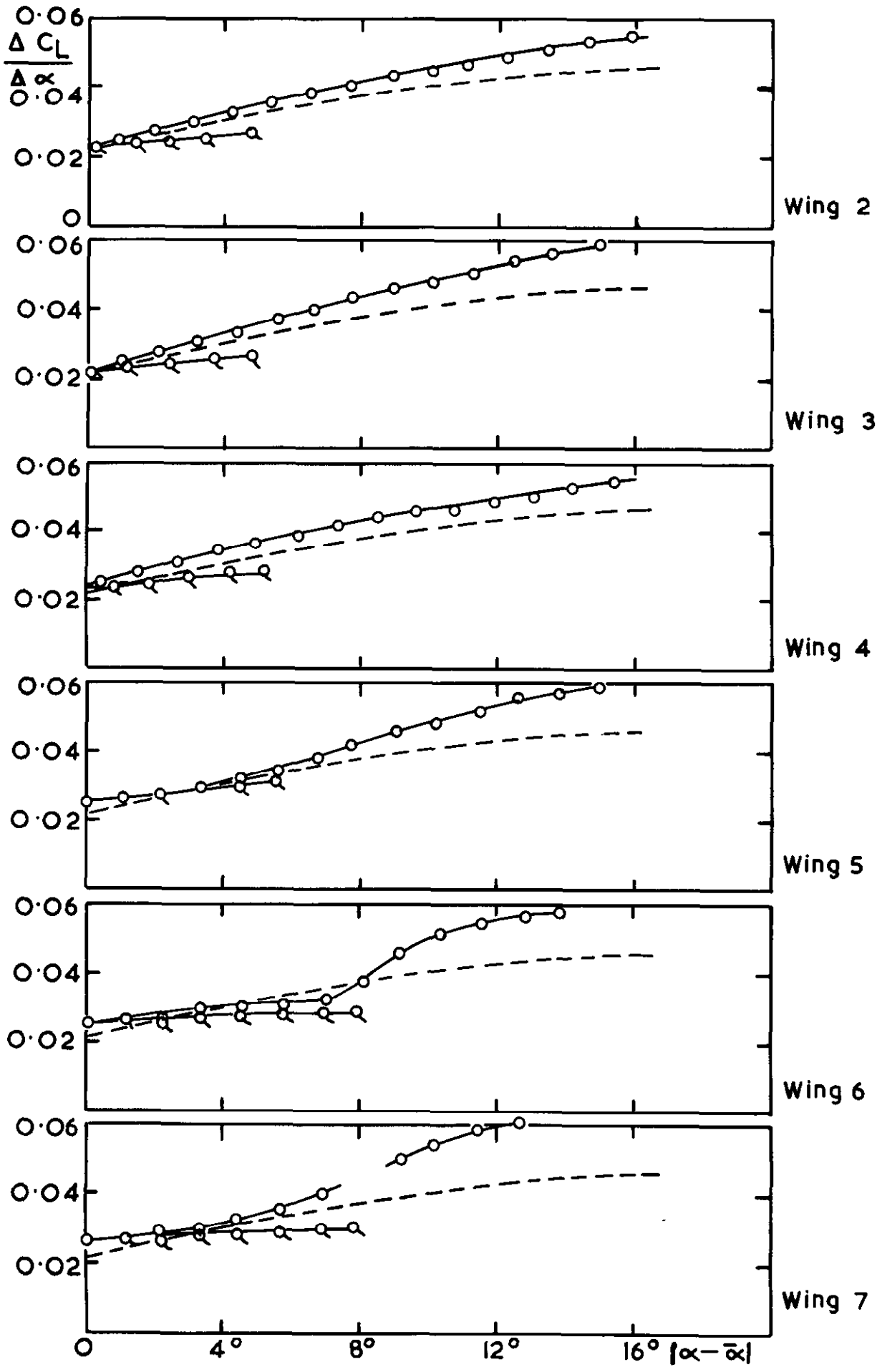

FIG. 7 $\frac{\Delta C_L}{\Delta \alpha}$ AGAINST $(\alpha - \bar{\alpha})$

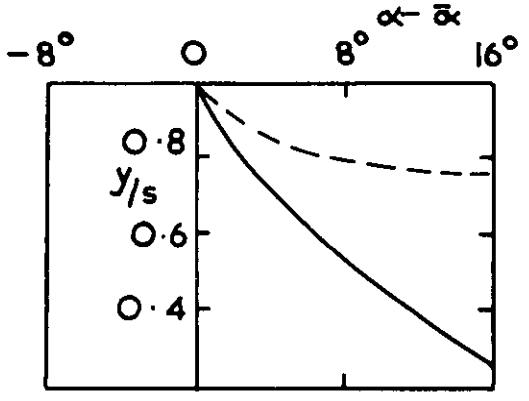

Wing 1

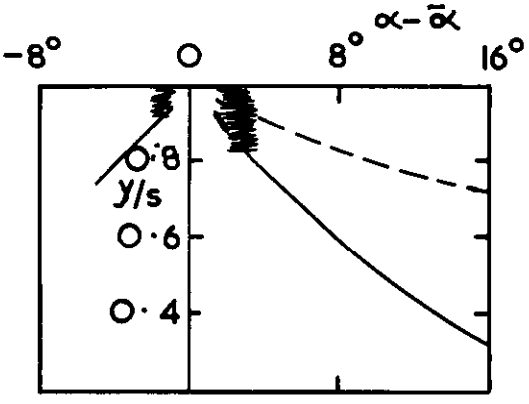

Wing 2

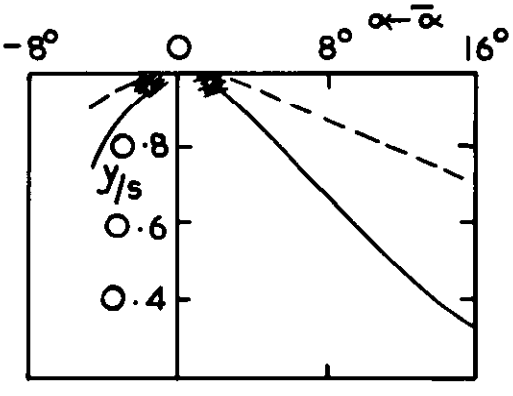

Wing 3

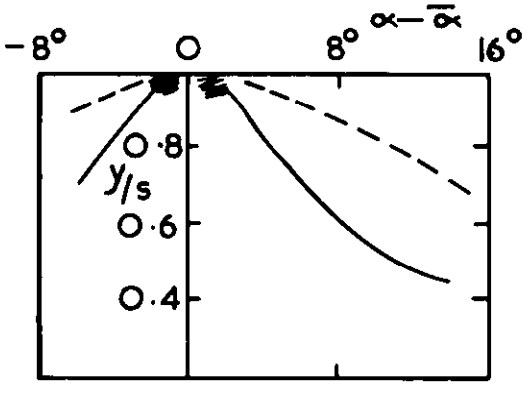

Wing 5

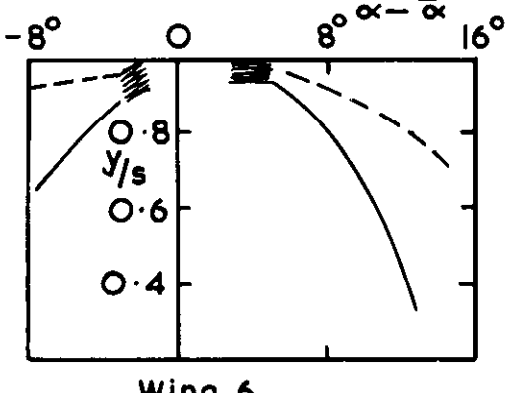

Wing 6

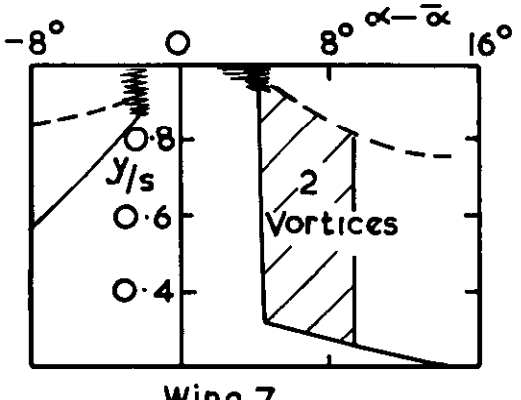

Wing 7

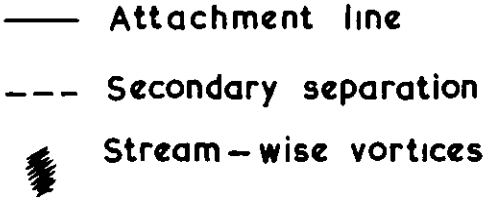

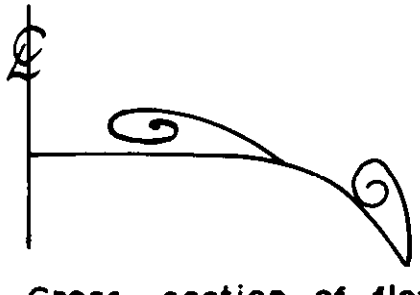

Cross-section of flow

Wing 7 $4.5° < (\alpha - \bar{\alpha}) < 9.7°$

FIG 8 SUMMARY OF SURFACE OIL-FLOW

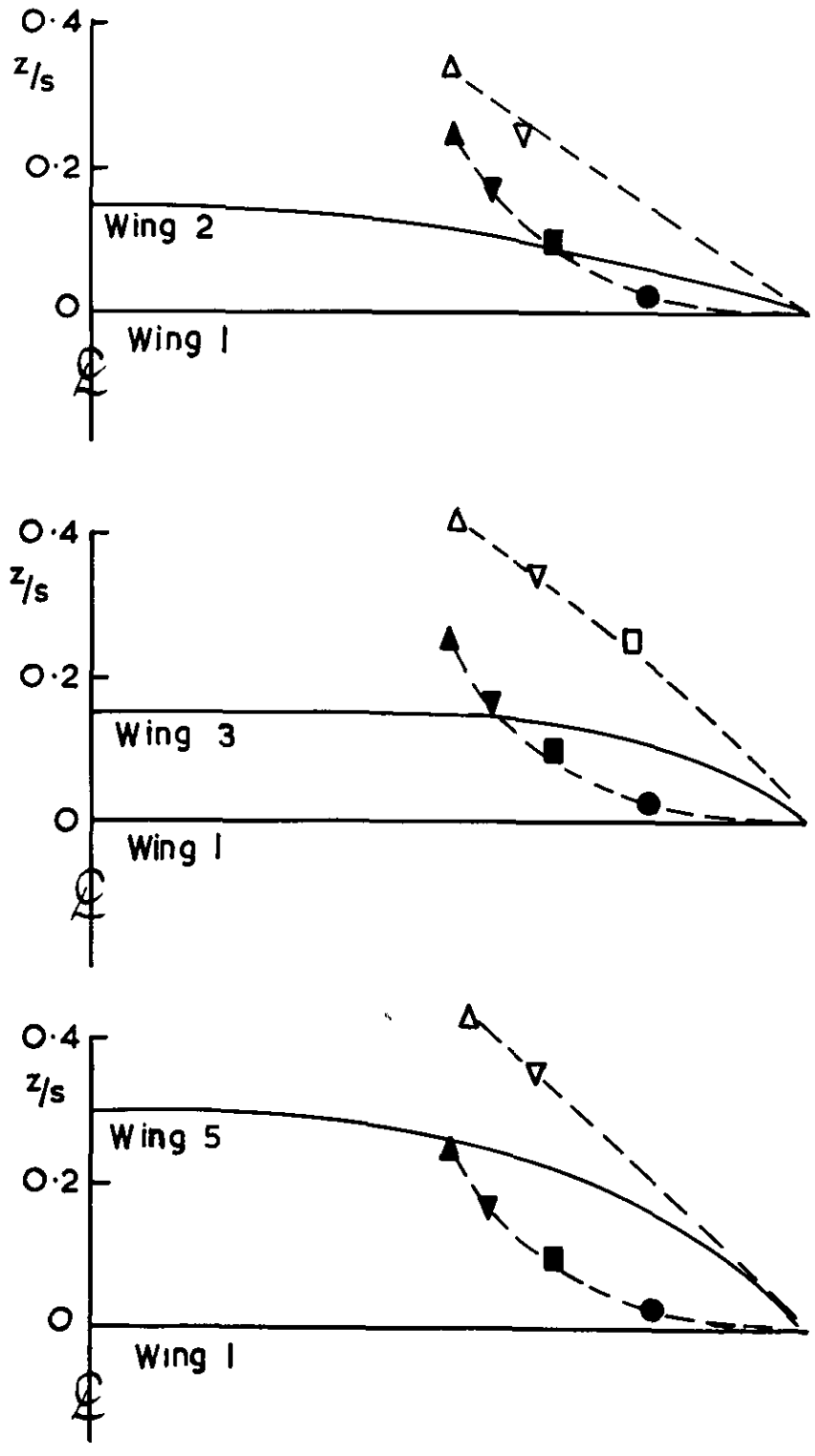

Δ $(\alpha - \bar{\alpha}) = 16°$
∇ $(\alpha - \bar{\alpha}) = 12°$
□ $(\alpha - \bar{\alpha}) = 8°$
○ $(\alpha - \bar{\alpha}) = 4°$

} Solid symbols for Flat wing

FIG. 9 VORTEX POSITIONS $(\frac{x}{c_o} \doteq 0{\cdot}8)$

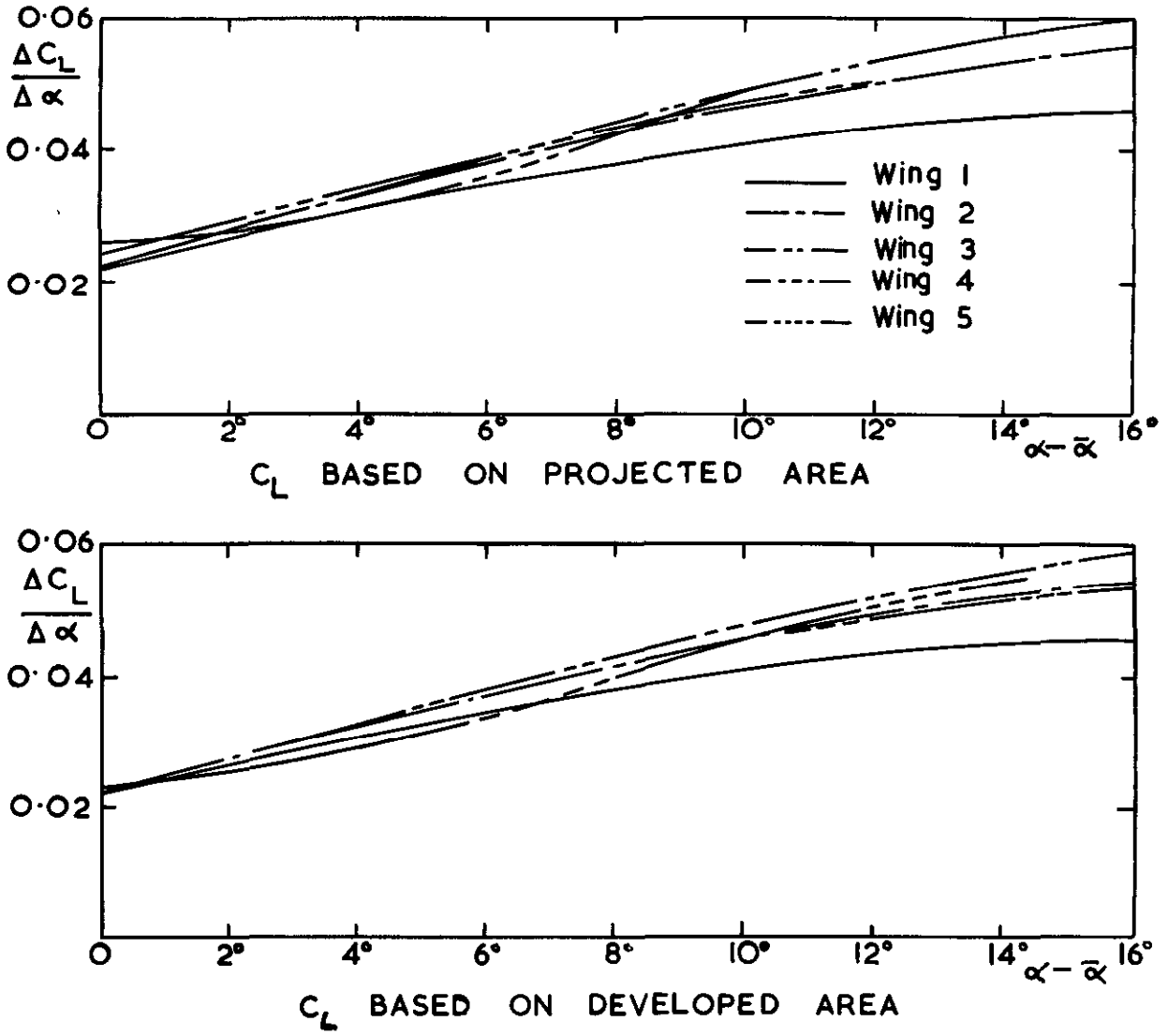

FIG. 10 COMPARISON OF CAMBERED WINGS

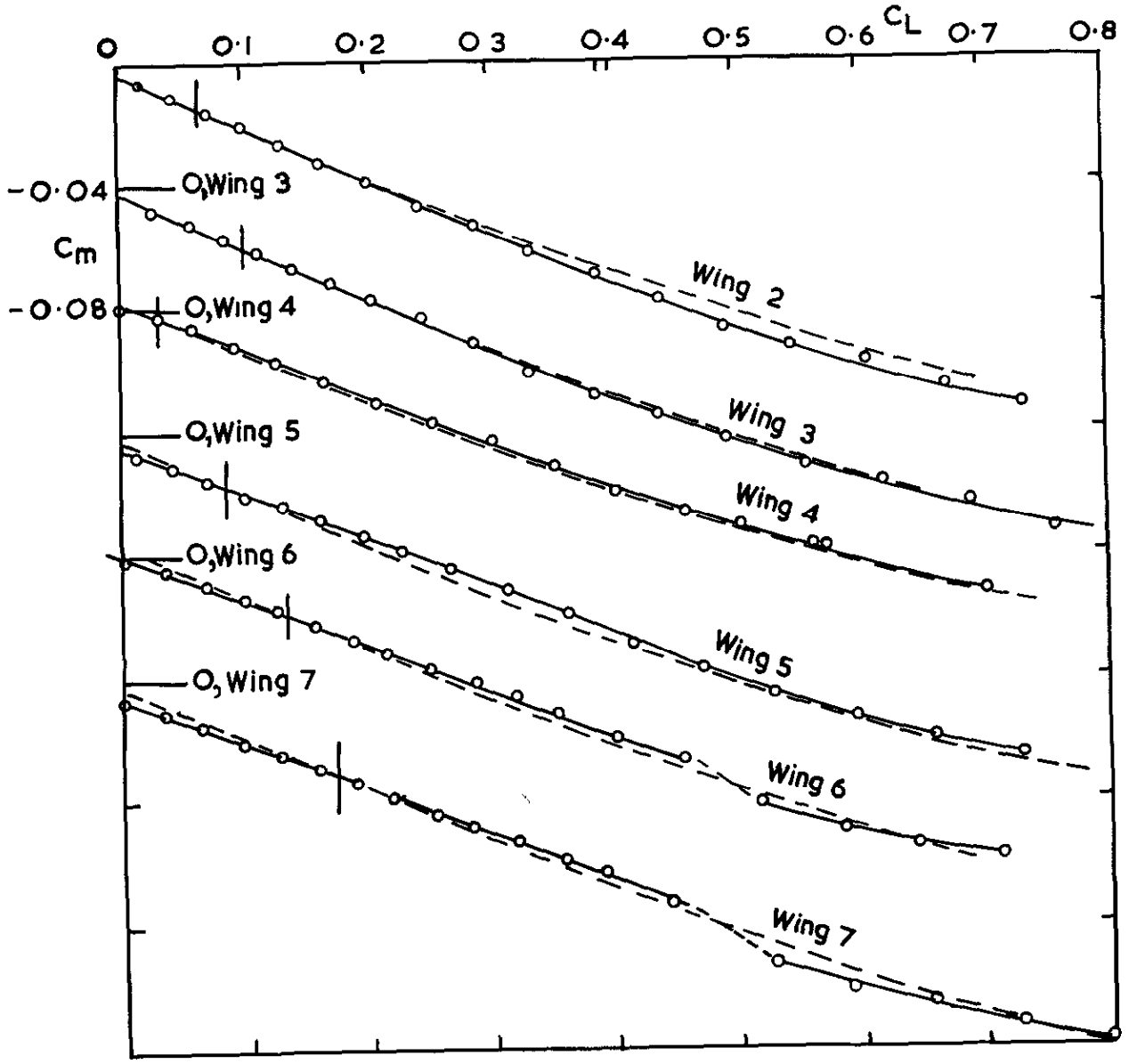

FIG 11 VARIATION OF C_m WITH C_L

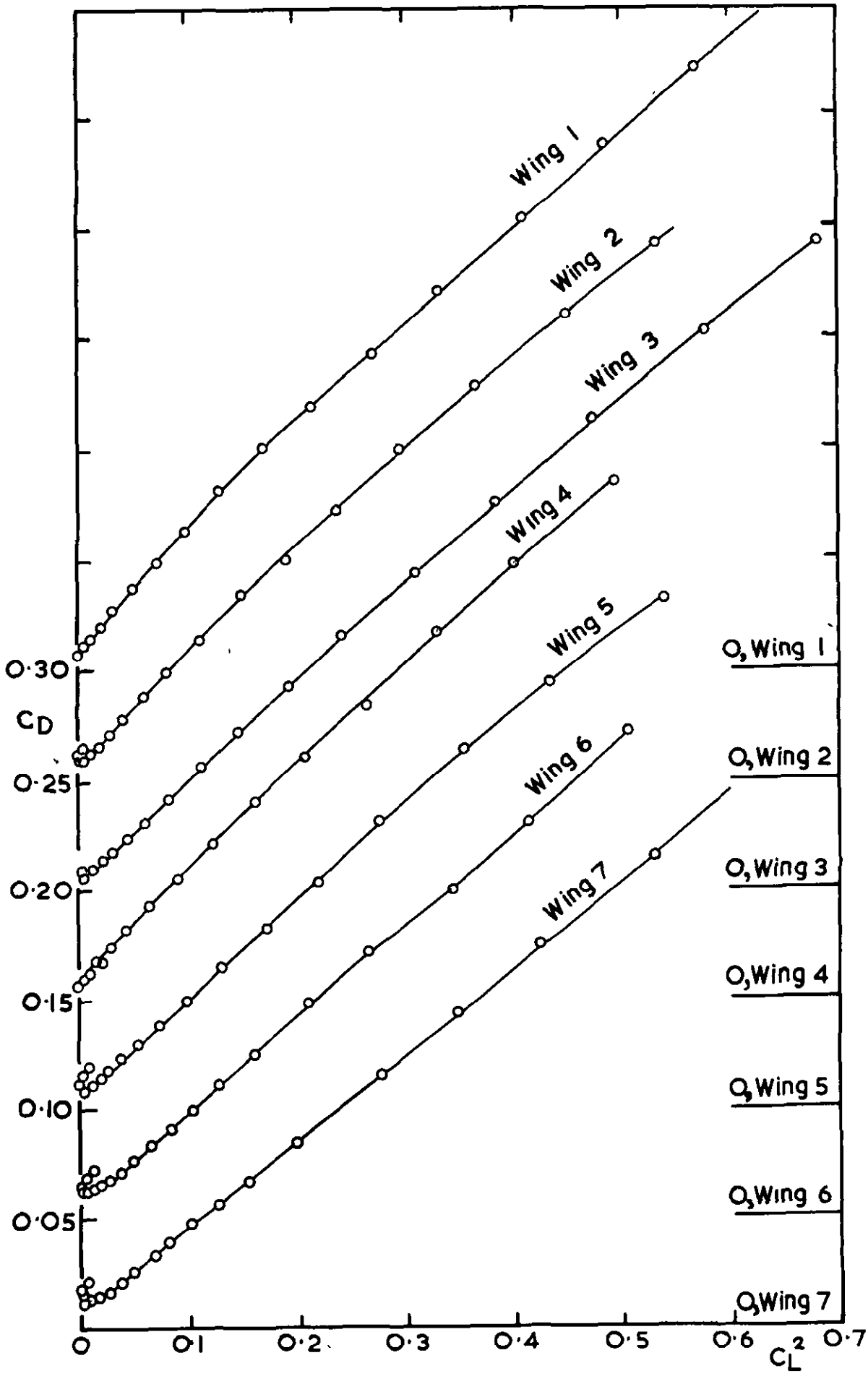

FIG 12. C_D AGAINST C_L^2

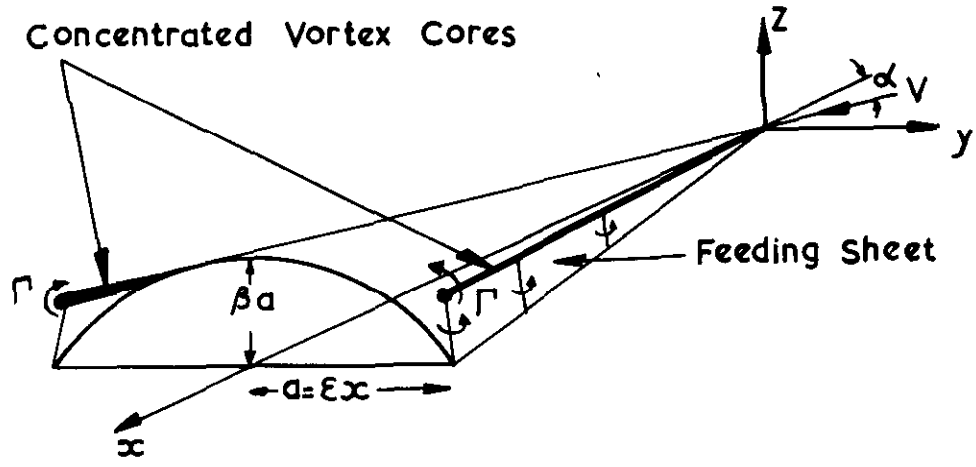

MATHEMATICAL MODEL AND NOTATION

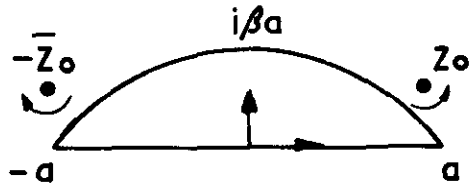

z – plane

$z_o = y_o + iz_o$

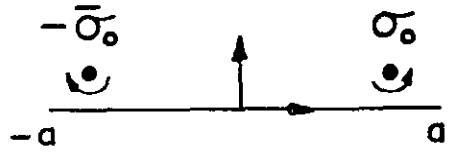

σ – plane

$\sigma_o = y_1 + iz_1$

$$\frac{\sigma}{a} = \frac{z - i\beta a}{a - i\beta z}$$

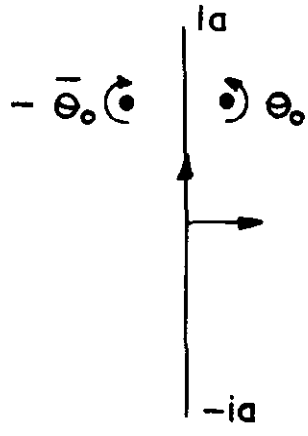

θ – plane

$\theta_o = y_2 + iz_2$

$\theta^2 = \sigma^2 - a^2$

FIG. 13. NOTATION

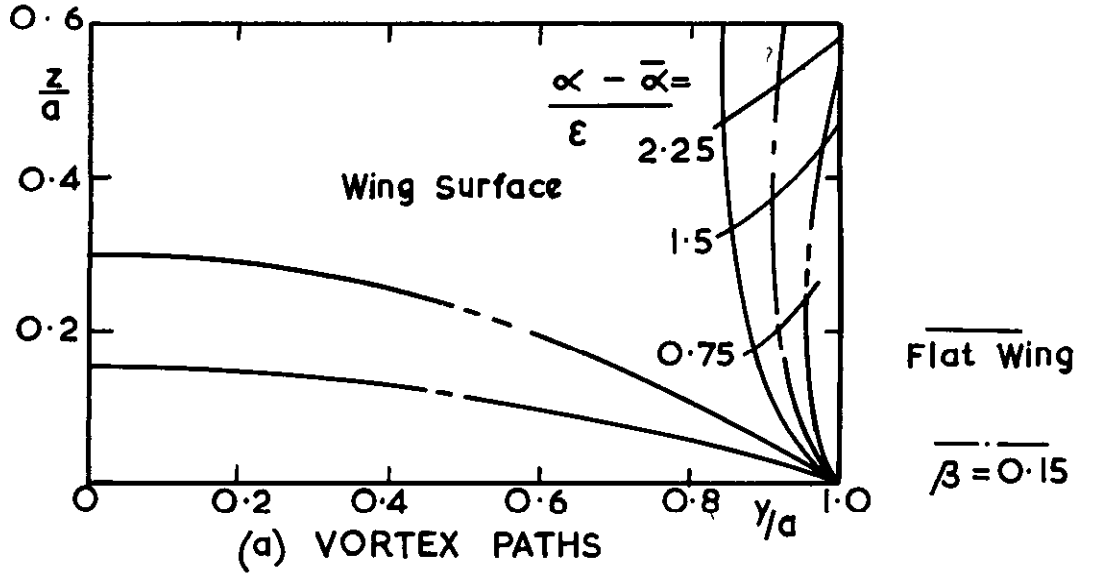

(a) VORTEX PATHS

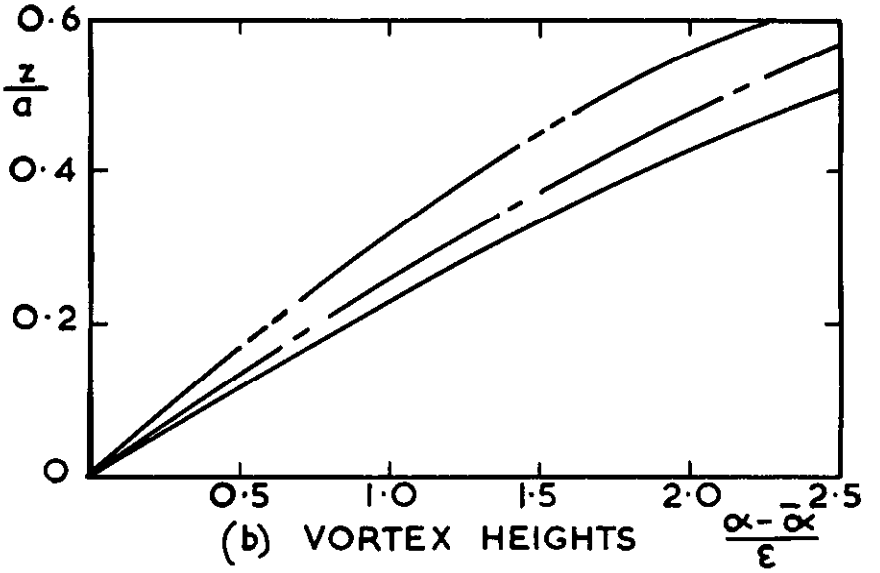

(b) VORTEX HEIGHTS

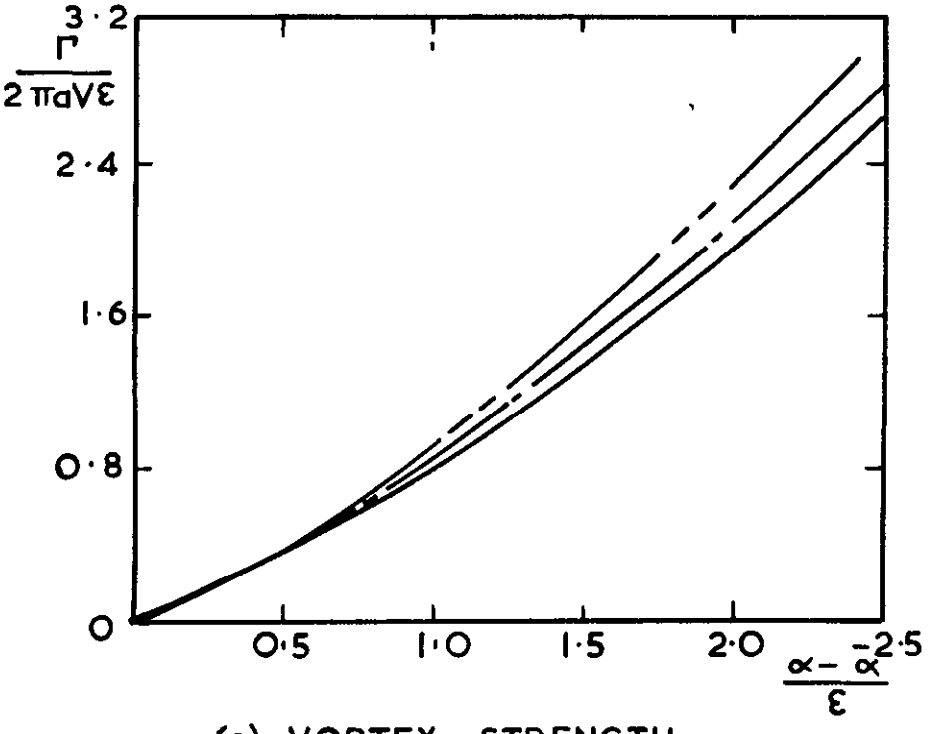

(c) VORTEX STRENGTH

FIG. 14 CALCULATED VORTEX POSITIONS AND STRENGTH

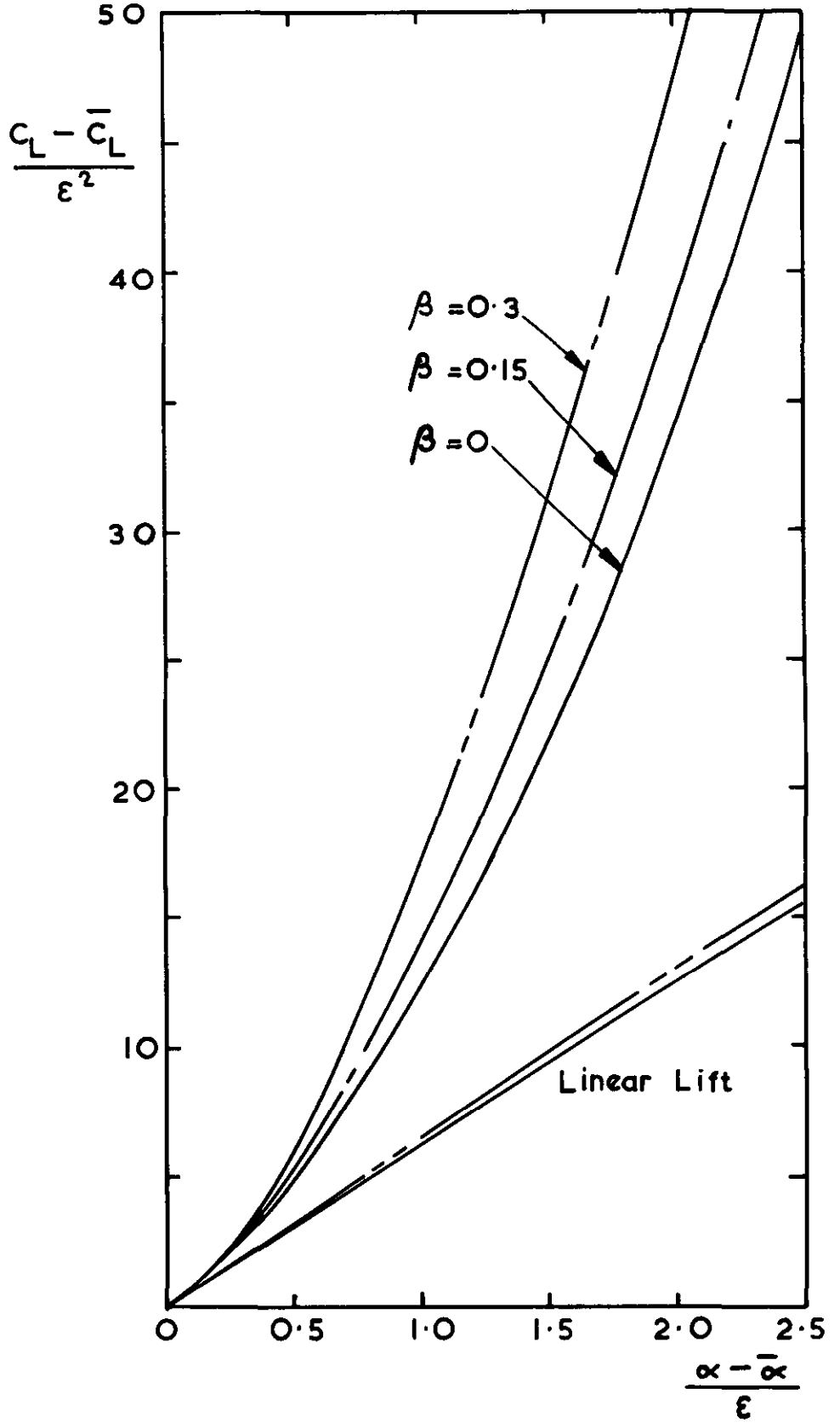

FIG. 15. CALCULATED LIFT

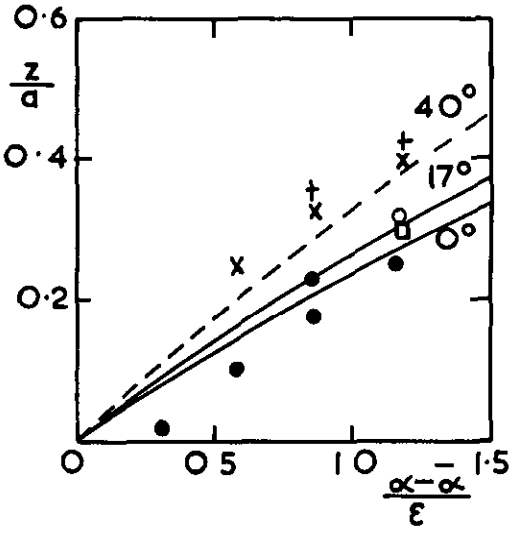

N.B. Z is height above leading edge

- ● Wing 1 $\phi = 0$ $\beta = 0$
- ○ Wing 2 $\phi = 16{\cdot}7°$ $\beta = 0{\cdot}15$
- × Wing 3 $\phi = 36{\cdot}8°$ $\beta = 0\ 15$
- □ Wing 4 $\phi = 16{\cdot}7°$ $\beta = 0\ 3$
- \+ Wing 5 $\phi = 42°$ $\beta = 0{\cdot}3$

FIG. 16 COMPARISON OF VORTEX HEIGHTS WITH THEORY

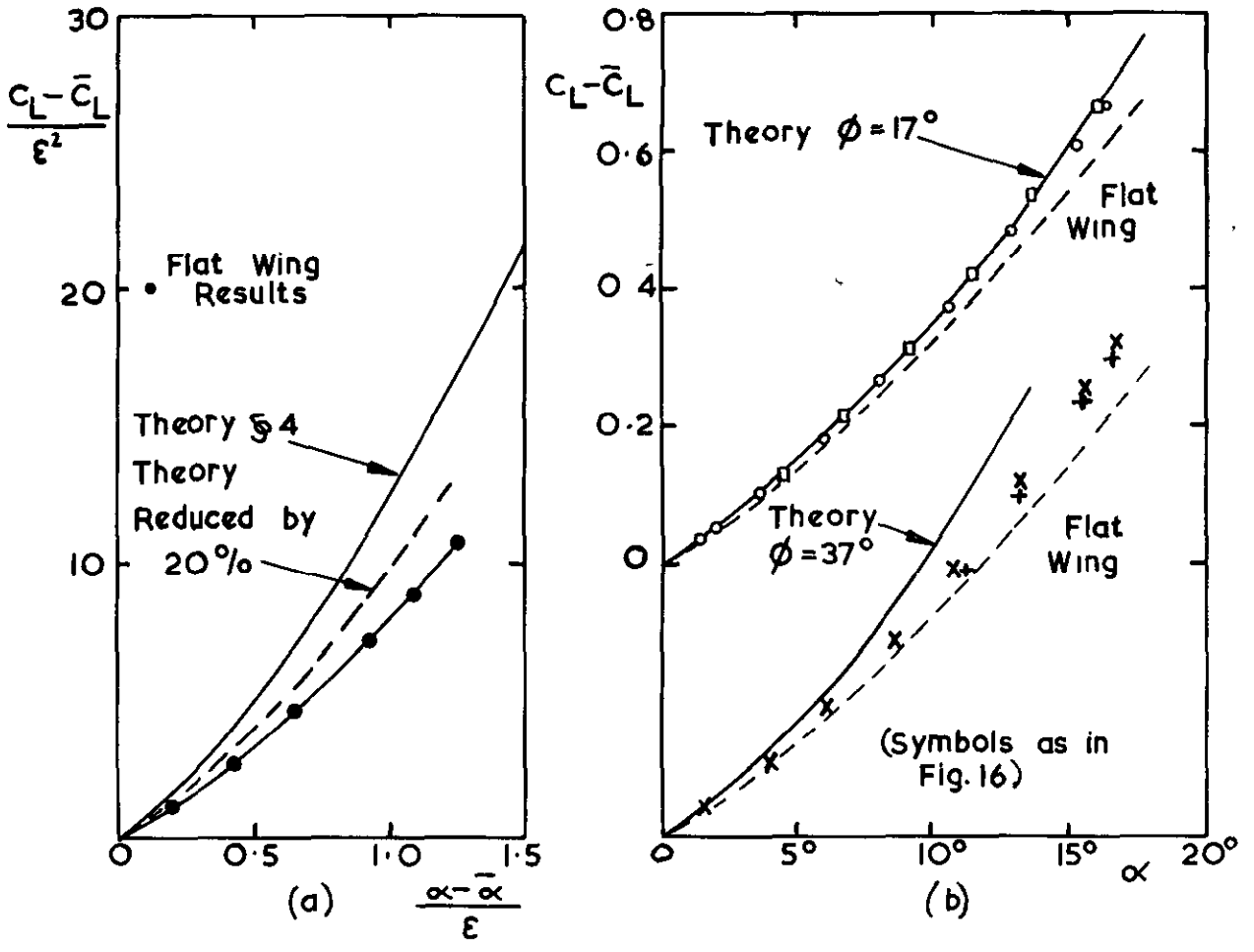

FIG 17 COMPARISON OF LIFT WITH THEORY

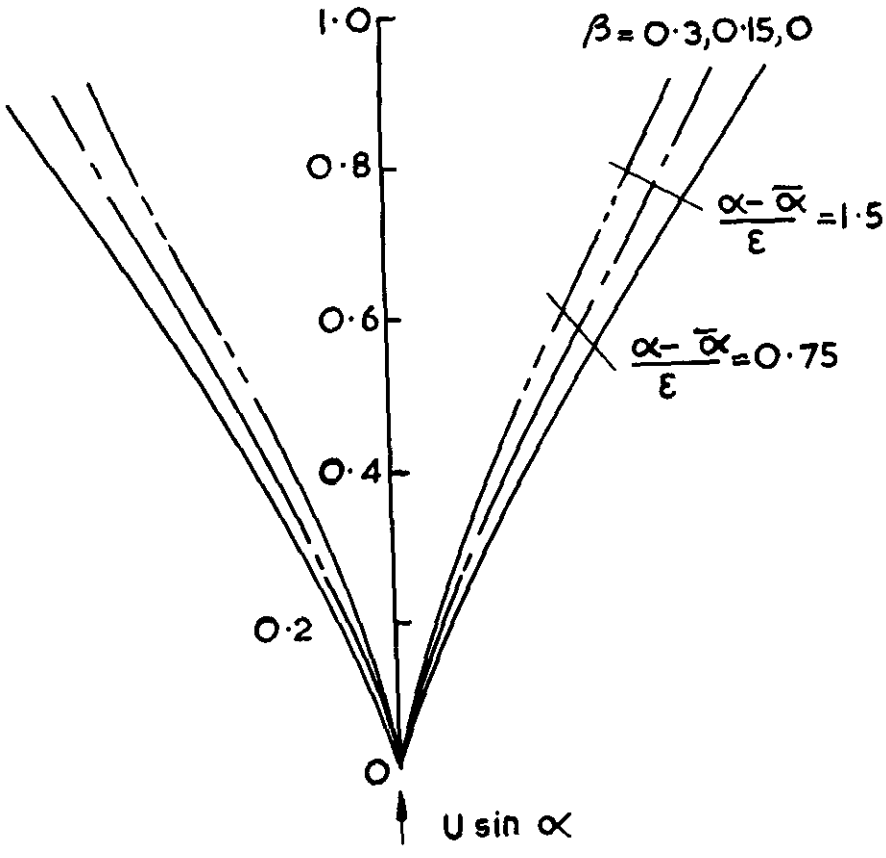

FIG. 18. VORTEX PATHS IN THE Θ PLANE (CIRCULAR ARC SECTIONS)

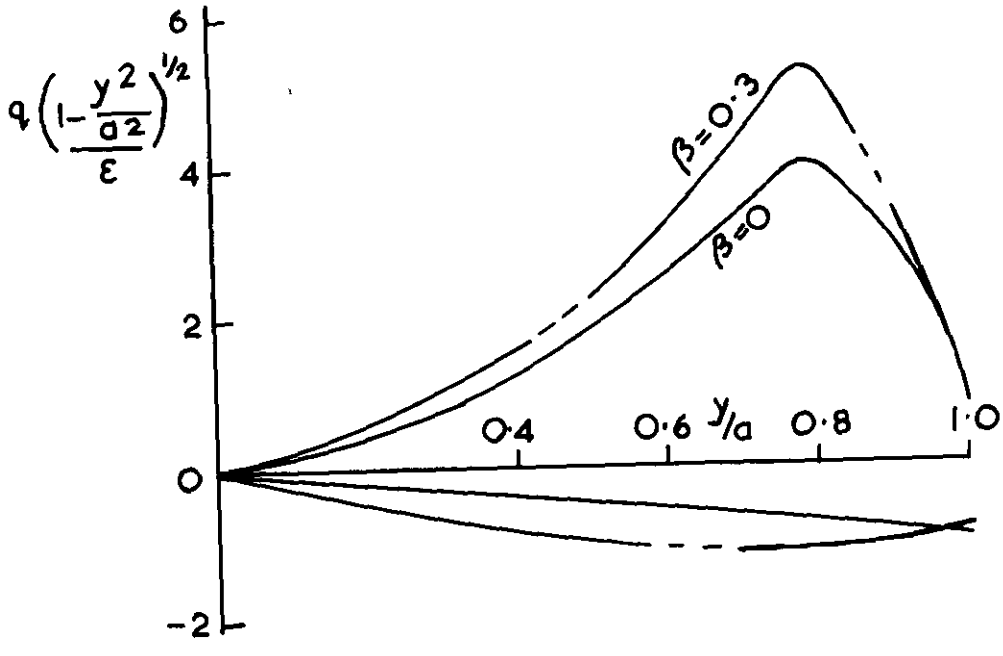

FIG. 19. CROSS FLOW VELOCITIES (CIRCULAR ARC SECTIONS)

A.R.C. C.P. No.924
18.1.66
Squire, L. C.

CAMBER EFFECTS ON THE NON-LINEAR LIFT OF SLENDER WINGS WITH SHARP LEADING EDGES

A study of published work on slender wings has shown that the non-linear lift is often increased by leading-edge droop. In this note the results are given of an investigation, made on simple, conically cambered wings, to study this effect in more detail. It is found that the main parameter which determines the increase in non-linear lift is the angle of droop at the leading edge. The magnitude of the increase, and the corresponding movements of the vortex positions, are predicted qualitatively by a simple extension to

A.R.C. C.P. No.924
18.1.66
Squire, L. C.

CAMBER EFFECTS ON THE NON-LINEAR LIFT OF SLENDER WINGS WITH SHARP LEADING EDGES

A study of published work on slender wings has shown that the non-linear lift is often increased by leading-edge droop. In this note the results are given of an investigation, made on simple, conically cambered wings, to study this effect in more detail. It is found that the main parameter which determines the increase in non-linear lift is the angle of droop at the leading edge. The magnitude of the increase, and the corresponding movements of the vortex positions, are predicted qualitatively by a simple extension to

A.R.C. C.P. No.924
18.1.66
Squire, L. C.

CAMBER EFFECTS ON THE NON-LINEAR LIFT OF SLENDER WINGS WITH SHARP LEADING EDGES

A study of published work on slender wings has shown that the non-linear lift is often increased by leading-edge droop. In this note the results are given of an investigation, made on simple, conically cambered wings, to study this effect in more detail. It is found that the main parameter which determines the increase in non-linear lift is the angle of droop at the leading edge. The magnitude of the increase, and the corresponding movements of the vortex positions, are predicted qualitatively by a simple extension to

DETACHABLE ABSTRACT CARDS

the Brown & Michael theory carried out for conically cambered wings with circular arc cross-sections. A study of the theoretical results shows that the principal cause of the increase in lift is the distortion of the velocity field of the vorticity which is produced by the curvature of the wing in the cross-flow plane.

the Brown & Michael theory carried out for conically cambered wings with circular arc cross-sections. A study of the theoretical results shows that the principal cause of the increase in lift is the distortion of the velocity field of the vorticity which is produced by the curvature of the wing in the cross-flow plane.

the Brown & Michael theory carried out for conically cambered wings with circular arc cross-sections. A study of the theoretical results shows that the principal cause of the increase in lift is the distortion of the velocity field of the vorticity which is produced by the curvature of the wing in the cross-flow plane.

Printed and published by
HER MAJESTY'S STATIONERY OFFICE

To be purchased from
49 High Holborn, London W C 1
423 Oxford Street, London W 1
13A Castle Street, Edinburgh 2
109 St Mary Street, Cardiff
Brazennose Street, Manchester 2
50 Fairfax Street, Bristol 1
35 Smallbrook, Ringway, Birmingham 5
7 - 11 Linenhall Street, Belfast 2
or through any bookseller

Printed in England

C.P. No. 924

S.O. Code No 23-9017-24